International Journal of Heat and Mass Transfer 180 (2021) 121743

Contents lists available at ScienceDirect

International Journal of Heat and Mass Transfer

journal homepage: www.elsevier.com/locate/hmt

Effect of low heat and mass fluxes on the boiling heat transfer coefficient of R-245fa

W.J. Van den Bergh[a], H.R. Moran[b], J. Dirker[a], C.N. Markides[b,c], J.P. Meyer[a,*]

[a] Department of Mechanical and Aeronautical Engineering, University of Pretoria, Pretoria, South Africa
[b] Clean Energy Processes (CEP) Laboratory, Department of Chemical Engineering, Imperial College London, London, U.K
[c] Kutateladze Institute of Thermophysics, Novosibirsk, Russian Federation

ARTICLE INFO

Article history:
Received 8 March 2021
Revised 26 June 2021
Accepted 12 July 2021

Keywords:
Flow boiling
Heat flux
Heat transfer
Mass flux

ABSTRACT

In-tube flow boiling at low mass and heat fluxes is of increasing interest particularly for low-concentration solar power systems, refrigerators, heat pumps, and other thermal management components and systems. In this study, the flow boiling of R-245fa was investigated experimentally for vapour qualities ranging from 0.05 to 0.90, mass fluxes of 40, 60 and 80 kg/m^{2}s, and heat fluxes of 2.5, 5.0 and 7.5 kW/m^2. Tests were done at quasi-steady-state conditions in a horizontal smooth tube with an inner diameter of 8.31 mm and a heated length of 0.8 m, at a saturation temperature of 35°C. It was found that the heat transfer coefficient was influenced by both the mass and heat fluxes. At any given vapour quality and heat flux combination, an increase in the mass flux resulted in an increase in the heat transfer coefficient. However, the magnitude of the increase and sensitivity to the mass flux was not the same in all of the test cases. Higher vapour quality cases were more sensitive to the mass flux than lower vapour quality cases, except at low heat flux conditions. In the most peculiar case, at the lowest considered heat flux of 2.5 kW/m^2, severe sensitivity to mass flux was observed at vapour qualities between 0.2 and 0.3. For all other heat fluxes, the heat transfer coefficient was found to be independent of the vapour quality except when the mass flux was high, where increased vapour quality resulted in improved heat transfer coefficients. Various correlations were investigated, but none of them captured the trends for the lowest heat flux.

© 2021 The Author(s). Published by Elsevier Ltd.
This is an open access article under the CC BY license (http://creativecommons.org/licenses/by/4.0/)

1. Introduction

Flow boiling has been an active field of research for several decades, with many studies investigating the effects of the fluid type, mass flux, heat flux, tube diameter and saturation conditions (temperature, pressure) on heat transfer performance. Fang et al. [1], for example, report that many studies on flow boiling have focussed on the range of mass fluxes between 100 and 600 kg/m^{2}s, and on heat fluxes above 5 kW/m^2, with over 60 correlations available to predict the heat transfer coefficient in these conditions. However, studies on flows with lower mass fluxes (below 100 kg/m^{2}s) and lower heat fluxes (below 5 kW/m^2), and of R-245fa specifically, are limited. Even rarer are studies of R-245fa in conventional tubes with a diameter greater than 3 mm, according to Kandlikar and Grande [2].

However, mass fluxes below 100 kg/m^{2}s and heat fluxes below 5 kW/m^2 are increasingly encountered in many applications, including common devices and systems such as domestic heat pumps or refrigerators, where the mass fluxes are typically below 60 kg/m^2 s and the heat fluxes below 2.5 kW/m^2 [3], as well as components such as plate heat exchangers [4]. Additionally, a recent surge in interest in low-concentration distributed organic Rankine cycle (ORC) power systems [5], as well as in distributed concentrated solar power (CSP) systems based on so-called direct steam generation (DSG), has elevated the interest specifically in these low mass and heat flux conditions, as well as in refrigerants such as R-245fa. DSG systems use the same fluid in the collector field as in the power cycle, and promise advantages relative to conventional indirect systems by eliminating the need for additional heat exchangers which, in traditional CSP plants, are used to transfer heat from the heat transfer fluid in the solar field to the working fluid in the power cycle [6], thus improving thermodynamic performance while lowering costs. In distributed (and, therefore, smaller-scale) [5] or hybrid solar (i.e., dual fuel/source) [7] systems,

* Corresponding author.
E-mail address: josua.meyer@up.ac.za (J.P. Meyer).

https://doi.org/10.1016/j.ijheatmasstransfer.2021.121743
0017-9310/© 2021 The Author(s). Published by Elsevier Ltd. This is an open access article under the CC BY license (http://creativecommons.org/licenses/by/4.0/)

Nomenclature

A: [m^2]	Area
Bi: [-]	Biot number
c_p: [J/kg K]	Isobaric specific heat capacity
d: [m]	Diameter
EB: [%]	Energy balance error
G: [kg/m^2 s]	Mass flux
h: [J/kg]	Specific enthalpy
I: [A]	Electric current
L: [m]	Length
k: [W/mK]	Thermal conductivity
$\dot{m}$: [kg/s]	Mass flow rate
$\dot{q}$: [W/m^2]	Heat flux
$\dot{Q}$: [W]	Heat transfer rate
T: [K,°C]	Temperature
V: [V or m^3]	Voltage or volume
x: [-]	Vapour quality

Special characters

α: [W/m^2 K]	Heat transfer coefficient

Subscripts

C	Characteristic, cross-sectional
cond	Condenser
Cu	Copper
f	Saturated liquid
fg	Difference between saturated liquid and saturated vapour
g	Saturated vapour
i	Inner
in	Inlet
m	Two-phase mixture
o	Outer
out	Outlet
pre	Preheater
ref	Refrigerant
s	Surface
n	Thermocouple station number along heated length
wall	Tube wall
test	Test section
tube	Copper tube
w	Water

the working fluid is often an organic fluid [8,9]. The reliable design and further development of these technologies necessitates a better understanding and improved prediction methods for the flow boiling of these refrigerants at relevant conditions. An overview of relevant literature follows.

Gómez Marzoa et al. [10] evaluated R-245fa in a horizontal smooth polyimide tube with an inner diameter of 2.689 mm at a mass flux ranging from 100 to 500 kg/m^2s, a heat flux from 15 to 55 kW/m^2, and saturation temperatures of 35, 41 and 47 °C. Boiling was achieved by hot water in an annulus around the test tube. It was found that a higher mass flux resulted in a higher heat transfer coefficient. At a mass flux of 100 kg/m^2 s, the vapour quality had a negligible effect on the heat transfer coefficient. The heat flux had no discernible effect, and it was hypothesised that the smoothness of the tube played a role. Increasing the saturation temperature had an almost negligible effect on the heat transfer coefficient at a mass flux of 200 kg/m^2s and heat flux of 15 kW/m^2, but at higher mass and heat fluxes (400 kg/m^2s and 45 kW/m^2), the heat transfer coefficient was lowered as the temperature increased.

Tibiriçá and Ribatski [11] evaluated flow boiling of R-134a and R-245fa for a horizontal stainless steel tube with an inner diameter of 2.3 mm and uniform joule heating. The mass fluxes considered ranged from 50 to 700 kg/m^2s, while the heat fluxes varied from 5 to 55 kW/m^2. The saturation temperatures were 22, 31 and 41°C. Higher mass fluxes resulted in higher heat transfer coefficients. However, increasing the vapour quality below a threshold mass flux of 200 kg/m^2 s had a detrimental effect on the heat transfer coefficient. At a mass flux of 100 kg/m^2 s and a heat flux of 15 kW/m^2, an increased saturation temperature resulted in an increased heat transfer coefficient. It was also found that an increased heat flux resulted in an increased heat transfer coefficient, regardless of the mass flux or fluid type under consideration.

Contributing to the flow-boiling database in microscale channels, Kanizawa et al. [12] evaluated the effect of saturation temperature, mass flux, hydraulic diameter and heat flux on the heat transfer coefficient of three fluids, R-134a, R-245fa and R-600a. For R-245fa, tests were conducted in tube sizes from 0.38 to 2.32 mm, at mass fluxes from 99 to 1 400 kg/m^2s, heat fluxes of 10 to 163 kW/m^2, and saturation temperatures of 25.5 to 58.3 °C. It was found that for R-245fa, for vapour qualities below 0.40, the heat transfer coefficient was markedly increased with higher heat flux, regardless of the tube diameter. The influence of saturation temperature was negligible at heat fluxes of 5 kW/m^2, but had the effect of a higher heat transfer coefficient at higher saturation temperatures at increased heat fluxes. The mass flux had a minimal effect on the heat transfer coefficient at qualities below 0.40, but as the vapour quality increased, the increased mass flux resulted in an increased heat transfer coefficient.

An extensive study was carried out by Da Silva Lima et al. [13] on R-134a in a smooth copper tube with an inner diameter of 13.84 mm for mass fluxes of 300 and 500 kg/m^2s, and heat fluxes of 7.5 and 15 kW/m^2. They considered saturation temperatures of 5, 15 and 20 °C and found that the heat transfer coefficient was higher for higher saturation temperatures at low vapour quality, but at higher vapour qualities, the opposite was true. The mass flux had a definite effect on the heat transfer coefficient, with the higher mass flux resulting in a higher heat transfer coefficient. The effect of this increase was amplified at higher vapour qualities. At low vapour qualities, higher heat fluxes resulted in higher heat transfer coefficients, but this effect was decreased at higher vapour qualities.

Dorao et al. [14] evaluated R-134a during flow boiling in a stainless steel tube with an inner diameter of 5 mm at a saturation temperature of 18.6 °C for mass fluxes between 200 and 400 kg/m^2s and heat fluxes between 3.9 and 47.1 kW/m^2. They found that the increased heat flux resulted in a higher heat transfer coefficient, regardless of the vapour quality. It also appeared that the highest heat flux had the effect of making the heat transfer coefficient independent of the mass flux and vapour quality. However, for lower heat fluxes, higher mass flux and vapour quality had the effect of increasing the heat transfer coefficient, with the effect of mass flux becoming more prominent at higher vapour qualities.

Celen and Dalkılıç [15] carried out a complete evaluation of the effects of mass flux, saturation temperature, heat flux and vapour quality on the heat transfer coefficient of R-134a in a tube with an inner diameter of 8.62 mm. They considered mass fluxes between 290 and 381 kg/m^2s, heat fluxes between 10.0 and 15.0 kW/m^2, and saturation temperatures between 15 and 22 C. It was found that the heat transfer coefficient increased with mass flux and vapour quality, due to the contribution of thinner liquid films and increased vapour velocity. This was more apparent at higher vapour qualities. Higher saturation temperatures resulted in higher heat transfer coefficients irrespective of the vapour quality range. At a mass flux of 290 kg/m^2s, increased heat fluxes resulted in

higher heat transfer coefficients, but this effect decreased for the higher mass flux of 381 kg/m^{2}s.

Grauso et al. [16] compared R-134a and R-1234ze(E). The thermodynamic properties of these two fluids are similar, with R-1234ze(E) having a lower global warming potential. This study included the effect of mass flux, heat flux, vapour quality and saturation temperature on the heat transfer coefficient obtained. The test section was a stainless steel tube with an inner diameter of 6 mm, with the test conditions covering mass fluxes between 146 and 520 kg/m^{2}s, heat fluxes of 5.0 to 20.4 kW/m^2, at saturation temperatures of -2.9 to 12.1°C. The heat transfer coefficient increased with vapour qualities, irrespective of the mass flux, although at higher mass fluxes, this was more pronounced. Higher mass fluxes resulted in higher heat transfer coefficients. The saturation temperature and heat flux were found to have a negligible effect on the heat transfer coefficient.

Bamorovat Abadi et al. [17] investigated the effect of gravity on the heat transfer and pressure drop of R-245fa by conducting tests in horizontal and vertical stainless steel tubes with inner diameter of 3 mm. The mass flux was ranged from 200 to 700 kg/m^{2}s for heat fluxes from 10.0 to 40.0 kW/m^2, while keeping the saturation temperature at 40 °C. Their data indicated that the heat flux had a relatively minor influence on the heat transfer coefficient, but was more pronounced at low vapour qualities. The mass flux had a much greater influence, with the heat transfer coefficient being higher at increased mass fluxes. Vertical tubes also exhibited a higher heat transfer coefficient than for horizontal tubes.

Bandarra Filho and Barbieri [18] evaluated the flow boiling performance of R-134a in horizontal microfin and smooth copper tubes. The inner diameters of the smooth tubes were 6.24 and 8.76 mm. The mass flux ranged between 100 and 500 kg/m^{2}s at a constant heat flux of 5.0 kW/m^2 and a saturation temperature of 5°C. The heat transfer coefficient increased with mass flux, but at values lower than 150 kg/m^2 s, it was unaffected by vapour quality in the smooth tube.

Manavela Chiapero et al. [19] investigated the boiling heat transfer coefficient of R-134a at 34°C in a smooth stainless steel tube with an inner diameter of 5 mm. They considered vapour qualities ranging from 0 to 1 for a mass flux between 300 and 500 kg/m^{2}s, and heat fluxes between 10.0 and 20.0 kW/m^2. It was found that for lower qualities, a higher heat flux corresponded to a higher heat transfer coefficient, and that this effect was more pronounced at the lower mass flux. The vapour quality had a negligible effect at the lower mass flux. Spindler and Müller-Steinhagen [20] also studied the flow boiling heat transfer of R-134a, and compared this to R-404a at low mass fluxes in a microfin tube as well as a smooth tube. The smooth tube had an inner diameter of 8.95 mm. Saturation temperatures of -20 to 0 °C were considered at mass fluxes of 25 to 150 kg/m^{2}s and heat fluxes of 1.0 to 15.0 kW/m^2. For R-134a, they found that at low mass and heat fluxes, the heat transfer coefficient was higher than expected. It was suggested that pool-boiling correlations be investigated for adapting correlations for enhanced tubes. The flow pattern was affected by the spiral grooves in the enhanced tube, which increased the wetted surface. A lower saturation temperature also resulted in a higher heat transfer coefficient.

The heat transfer coefficients in flows of R-134a and R-404A were compared for saturation temperatures ranging from -15 to 0 °C in a tube with an inner diameter of 7.49 mm by Balachander and Raja [21]. Mass fluxes ranged between 57 and 102 kg/m^{2}s and the heat flux for R-134a was between 7.5 and 8.3 kW/m^2. An increased mass flux resulted in a higher heat transfer coefficient. Increasing vapour quality had a detrimental effect on the heat transfer coefficient, as did increasing the saturation temperature. It was concluded that this was due to the flow pattern being stratified wavy instead of annular.

Björk and Palm [22] studied the boiling heat transfer in a domestic plate-type evaporator using R-600a as refrigerant, with the presence of frequent bends and a non-circular cross-section with a hydraulic diameter of 3.21 mm. The mass flux varied from 21 to 43 kg/m^{2}s, and the heat flux from 1.0 to 5.0 kW/m^2, while the temperature under consideration was -15°C. The heat transfer coefficient decreased with increasing vapour quality and heat flux at the lowest mass flow rate tested. For higher mass flow rates, the heat transfer coefficient increased with increased vapour quality, but was largely independent of applied heat flux. The achieved heat transfer coefficient was higher than that predicted by correlations, and it was hypothesised that the flow pattern contributed to this discrepancy.

A study covering a fairly wide range of conditions for refrigerants R-22, R-134a and R-404a was conducted by Saiz Jabardo and Bandarra Filho [23] in a copper tube with an inner diameter of 12.7 mm. These conditions consisted at temperatures of 8 and 15 °C, mass fluxes of 50 to 500 kg/m^{2}s, and a heat flux of between 5 and 20 kW/m^2. It was found that for low mass fluxes, the heat transfer coefficient was only weakly dependent on the vapour quality, and in fact decreased slightly for higher qualities. However, the heat flux had an effect on the heat transfer coefficient throughout the quality range at low mass fluxes, and at lower qualities at higher mass fluxes. At mass fluxes above 200 kg/m^{2}s, the flow pattern transitioned from stratified to annular, and the heat transfer coefficient increased with increasing quality up to dryout. The saturation temperature had a positive effect on heat transfer at lower qualities.

Wattelet et al. [24] found that for lower mass fluxes, the heat transfer coefficient was also largely independent of vapour quality, but was affected to a sizable degree by the heat flux being tested. They compared experimental heat transfer coefficients for flow of R-134a, MP-39 and R-12. The mass fluxes under consideration were from 25 to 100 kg/m^{2}s, at saturation temperatures of -15 to 5 °C and heat fluxes of 2.0 to 10.0 kW/m^2. Their test facility consisted of a smooth copper tube with an inside diameter of 7.04 mm. Increasing mass and heat flux resulted in an increased heat transfer coefficient.

The results of the studies presented in this work thus far are summarised in Table 1. The reported results of increased saturation temperature (T_{sat}), mass flux (G), heat flux ($\dot{q}$) and vapour quality (x) are indicated to either increase (↑) or decrease (↓) the heat transfer coefficient. There is consensus in the literature about the heat transfer coefficient being highly dependent on mass flux, but no consensus on the effect of vapour quality, saturation temperature and heat flux. Gómez Marzoa et al. [10] found that the effect of increasing heat flux on the heat transfer coefficient was mild. Björk and Palm [22] observed that increasing heat flux had a negative effect on the heat transfer coefficient. The rest of the literature reviewed reported that increasing the heat flux had a significant positive effect on the heat transfer coefficient, either throughout the vapour quality range and mass fluxes tested, or at least for lower vapour qualities. The effect of increasing vapour quality was noted by Gómez Marzoa et al. [10] to be negligible at a mass flux of 100 kg/m^{2}s, while Saiz Jabardo and Bandarra Filho [23] found that at mass fluxes of 50 and 100 kg/m^{2}s, the increase in vapour quality actually had a negative effect on the heat transfer coefficient. The other studies found that for mass fluxes above 200 kg/m^{2}s, the increase in vapour quality corresponded to an increased heat transfer coefficient. Of interest is that Manavela Chiapero et al. [19] only observed this for a mass flux of 500 kg/m^{2}s.

These findings must be viewed in the light of the two main contributors to flow boiling, that of convective and nucleate boiling. Convective boiling dominates when the mass flux is sufficiently high, which means the flow pattern becomes annular at very low vapour qualities. As the vapour quality increases, the heat

Table 1
Overview of studies of in-tube boiling of refrigerants at low mass and heat fluxes.

Author(s)	Fluid	Experimental apparatus	T_{sat} [°C]	G [kg/m^{2}s]	$\dot{q}$ [kW/m^2]	Effect of increase on α
Gómez Marzoa et al. [10]	R-245fa	2.689 mm, horizontal smooth, non-uniform heat flux	35 to 47	100 to 500	15.0 to 55.0	T_{sat}: Negligible G: ↑ $\dot{q}$: Negligible x: Negligible at 100 kg/m^{2}s
Tibiriçá and Ribatski [11]	R-134a R-245fa	2.3 mm, horizontal smooth, uniform heat flux	22 to 41	50 to 700	5 to 55	T_{sat}: ↑ for 100 kg/m^2 s and 15.0 kW/m^2 G: ↑ $\dot{q}$: ↑ x: ↑ for >200 kg/m^{2}s
Kanizawa et al. [12]	R-134a R-245fa R-600a	0.38-2.6 mm inner diameter, horizontal smooth tubes, joule heated	25.5 to 58.3	99 to 1400	10 to 163	T_{sat}: ↑ for $\dot{q}$>5 kW/m^2 G: ↑ for x>0.40 $\dot{q}$: ↑ for x <0.40
Da Silva Lima et al. [13]	R-134a	13.84 mm inner diameter, horizontal smooth tube, counterflow boiled	5 to 20	300 to 500	7.5 to 17.5	T_{sat}: ↑ for lower x; ↓for higher x G: ↑ $\dot{q}$: ↑ at lower x
Dorao et al. [14]	R-134a	5.00 mm inner diameter, horizontal smooth tube, joule heated	18.6	200 to 400	3.9 to 47	G: ↑ $\dot{q}$: ↑; independent of G and x if high enough x: ↑
Celen and Dalkılıç [15]	R-134a	8.62 mm inner diameter, horizontal smooth tube, electrical resistance heated	15 to 22	290 to 381	10 to 15	T_{sat}: ↑ G: ↑ $\dot{q}$: ↑; less of an effect at high G
Grauso et al. [16]	R-134a R-1234ze(E)	6 mm inner diameter, horizontal smooth tube, joule heated	-2.9 to 12.1	146 to 520	5 to 20.4	T_{sat}: Negligible G: ↑ $\dot{q}$: ↑ for x < 0.2
Bamorovat Abadi et al. [17]	R-245fa	3 mm inner diameter, horizontal and vertical smooth tube, joule heated	40	200 to 700	10 to 40	G: ↑ $\dot{q}$: ↑ for lower G and lower x
Bandarra Filho and Barbieri [18]	R-134a	8.76 mm inner diameter, horizontal smooth, herringbone and microfin tube, electrical resistance heated	5	100 to 500	5	G: ↑ $\dot{q}$: Single heat flux investigated x: ↑ for G>100 kg/m^{2}s
Manavela Chiapero et al. [19]	R-134a	5 mm internal diameter, horizontal smooth tube, joule heated	34	300 to 500	10 to 20	G: ↑ $\dot{q}$: ↑ at low x x: ↑ for G=500 kg/m^{2}s
Spindler and Müller-Steinhagen [20]	R-134a R-404A	9.52 mm outer diameter, horizontal smooth and microfin tube, electrical resistance heated	-20 to 10	25 to 150	1 to 15	T_{sat}: ↑ except for -20°C G: ↑ $\dot{q}$: ↑ for low x
Balachander and Raja [21]	R-134a R-404A	7.49 mm inner diameter, horizontal smooth tube, counterflow acetone heated	-15 to 0	57 to 102	2 to 18	T_{sat}: ↓ for low G G: ↓ for lower x
Björk and Palm [22]	R-600a	Cut section of a plate-type evaporator with hydraulic diameter 3.21 mm, electrical resistance heated	-15	21 to 43	1 to 5	G: ↑ $\dot{q}$: ↓ for G=21 kg/m^2 s x: ↑ for G>21 kg/m s
Saiz Jabardo and Bandarra Filho [23]	R-22 R-134a R-404A	12.7 mm inner diameter, horizontal smooth tube, electrical resistance heated	8 to 15	50 to 500	5 to 20	T_{sat}: ↑ for $\dot{q}$ ≥20 kW/m^2 G: ↑ $\dot{q}$: ↑ x: ↓ for G=50 and 100 kg/m^{2}s
Wattelet et al. [24]	R-134a R-12 MP-39	7.04 and 10.92 mm inner diameter, horizontal smooth tube, electrically heated	-15 to 5	25 to 100	2 to 10	G: ↑ $\dot{q}$: ↑ for lower G

transfer coefficient also increases, since the annular film thickness becomes thinner. Nucleate boiling, on the other hand, depends on the bubble formation rate, nucleation sites (which depend on the pipe roughness), and the applied heat flux. This boiling mechanism dominates when the mass flux is low enough, and the flow patterns are thus stratified in some form throughout the vapour quality range. The mass flux at which nucleate boiling dominates over convective boiling is thus of particular interest.

While there are examples of condensation studies of macrotubes at low mass fluxes [25], boiling studies of mass fluxes under 100 kg/m^{2}s and heat fluxes below 5.0 kW/m^2 have received less attention. This is illustrated in Fig. 1, which also presents the focus area of this study.

No consensus has been reached on the effect of various adjustable experimental factors on the heat transfer coefficient at these conditions, and there are no guidelines for predicting the heat transfer coefficient by using correlations. Moran et al. [26] assessed the performance of heat transfer coefficient predictive methods for R-245fa boiling in a 12.6 mm horizontal pipe at heat and mass flux conditions from 30 to 700 kg/m^{2}s and 0.5 to 38 kW/m^2 respectively, and found correlations to give less accurate predictions at low vapour qualities which were typically associated with low heat flux conditions in their experiments. For this subset of their data where nucleate boiling was expected to be the dominant heat transfer mechanism, Moran et al. [26] also assessed the applicability of pool boiling predictive methods but found them to give low accuracy when compared to experimental heat transfer coefficient values. It is therefore the purpose of this study to partially narrow this gap by investigating flow boiling for R-245fa in a horizontal smooth tube with an inner diameter of 8.31 mm. This

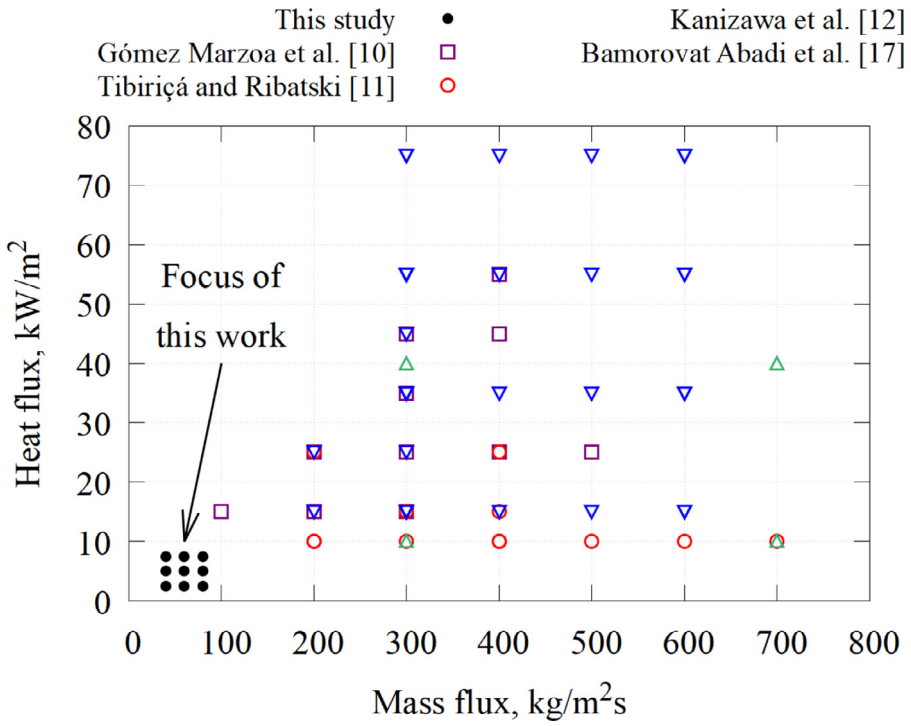


Fig. 1. Focus of this work and relevance to other existing studies on the flow boiling of R-245fa.

refrigerant, along with the tube diameter, was chosen because it has actively been studied for use in small-scale organic Rankine cycles [5]. The mass fluxes that were investigated were 40, 60 and 80 kg/m^{2}s, with a heat flux of 2.5, 5.0 and 7.5 kW/m^2. These were informed by the mass fluxes in plate heat exchangers [4] and domestic refrigerators [3]. The vapour qualities studied ranged from 0.05 to 0.90.

2. Experimental apparatus

2.1. Facility

The apparatus used in this study was a closed R-245fa refrigerant loop, shown schematically in Fig. 2. This loop was also utilised by Dirker et al. [27], where the interested reader can find further details on the facility, apparatus and methods. This refrigerant was stored in a liquid receiver, which was connected to a fixed-displacement, variable-frequency gear pump. This pump was used to drive the refrigerant through the electrically heated preheater (located between Points A and B) and test section (located between Points C and D), before it passed through a water-cooled condenser and back to the liquid receiver. The main line of the fluid circuit included the mass flow meter, while an additional bypass line with a needle valve was used to finely control the mass flow rate through the main line.

A smooth hard-drawn copper tube with an outside diameter of 12.7 mm was used to construct the entire facility, barring the test section. The liquid receiver was placed roughly 1.5 m above the pump suction side, and had a capacity of 18 L. This was done to guarantee a liquid state of the fluid at pump entry, due to the pressure difference. The capacity of the liquid receiver also acted as a temperature buffer.

The gear pump was a magnetically coupled, variable-frequency GATHER pump with minimum and maximum rated flow rates of 14.4 and 540 L/h respectively. The mass flow meter was a Micro-Motion CMF010 Coriolis flow meter, with a maximum rated range of 0.04 kg/s, and an accuracy of 0.1%.

In order to heat the fluid to saturation conditions, and to control the vapour quality entering the test section, heat was added to the fluid in the preheater, which consisted of high resistance electrically insulated constantan wire tightly coiled around two 1.9 m long copper tubes with an outer diameter of 12.7 mm. The electrical insulation between the wires, as well as the copper pipe, was confirmed by use of a multimeter. The resistance for each of the wires was 35 Ω, and the wires were connected individually to two ElektroAutomatik EA8360-30 DC power supply units, rated at 3 kW each. The accuracy of these power supply units was 0.2% of the output voltage and current.

The same method was used to provide the heat flux in the test section for the flow-boiling experiments. The test section, discussed in more detail in the next section, was powered by an ElektroAutomatik EA8360-15 DC power supply with a rating of 1.5 kW. Its accuracy was the same as the power supply units used in the preheater. The linear distance between the preheater exit and test section entry was 3.5 m.

In order to ensure full liquid condensation before returning to the receiver, a water-cooled condenser was used. The water source was a Lauda thermal bath with a water capacity of 35 L and a cooling capacity of 800 W. The internal pump of the thermal bath circulated water through the condenser and through a Coriolis flow meter, which was a MicroMotion CMF025 flow meter, with a maximum range of 0.4 kg/s, and an accuracy of 0.1%. A three-way valve was also installed on the water line to enable flow rate control above and beyond the eight power levels provided by the thermal bath internal pump.

For data collection and control purposes, key points were instrumented with temperature sensors, denoted by **T** in Fig. 2, and absolute pressure transducers, denoted by **P**. The absolute pressure transducers mounted before and after the gear pump were GEMS 2200 series transducers, while Sensotec FP2000 transducers were utilised on the rest of the facility. The accuracy of these sensors was 0.2% of full scale and 0.25% respectively. All pressure transducers were mounted to the system using pressure taps. These taps were drilled to a diameter of 0.8 mm, at a horizontal level. In or-

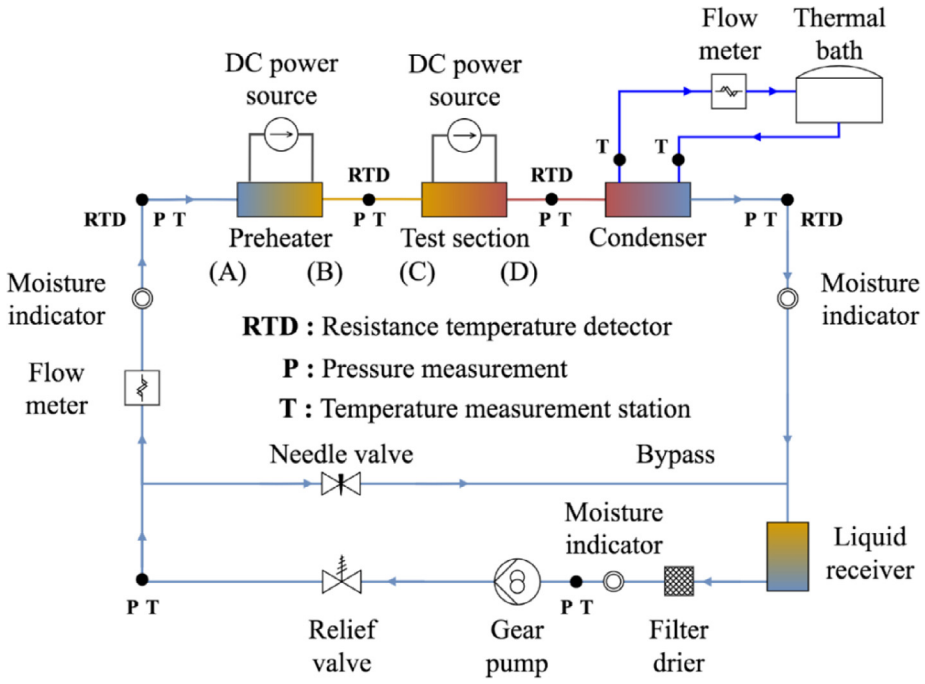


Fig. 2. Experimental test facility schematic.

der to minimise the flow disturbance introduced by these taps, the diameter of the holes was kept to below a tenth of the tube diameter. Furthermore, they were deburred carefully to minimise this disturbance.

Four T-type thermocouples, mounted circumferentially equidistant around the tube, were present at each temperature measuring station marked with a **T** in Fig. 2. Thermal tape was used to secure the thermocouples in place. These thermocouples had an accuracy of 0.1 °C. In order to ensure correct thermocouple readings, and provide monitoring to the system, resistance temperature detectors (RTDs) were also used. These are indicated by **RTD** in Fig. 2, and were 1/10 DIN Omega Pt100s with an accuracy of 0.03 °C. Their measuring tips were mounted to be completely surrounded by the fluid.

To ensure minimal energy losses, thermal insulation with a stated thermal conductivity of 0.036 W/mK was applied to the entire facility. The minimum radius of this insulation was 80 mm.

2.2. Test section

The test section consisted of a calming section, an inlet sight glass for visual observation of the flow pattern, a monitored length and an outlet sight glass, as represented schematically in Fig. 3.

The monitored length was equipped with a large number of thermocouples as described later, and consisted of a smooth hard-drawn copper tube with an outer diameter (d_o) of 9.53 mm, an inner diameter (d_i) of 8.31 mm, and a total length of 1 m. Of this, a section with a length of 0.8 m (L_h) was electrically heated via a resistance wire of the same type as that used in the preheater that was tightly wound around the circumference for the entire length L_h. This wire had a nominal resistance of 180 Ω. This enabled a uniform circumferential heat flux to be applied to the test section.

The upstream calming section had the same diameter as the monitored section and was 0.5 m in length (approximately 60 times d_i). Its purpose was to reduce untoward effects on the flow pattern caused by upstream components and flow passage elbows. Its length was selected based on the findings of Cho and Tae, as reported in Ref. [28], namely that the influence of upstream bends on the observed flow characteristic was present for a distance of up to 48 times the internal diameter of the tube.

The sight glasses were manufactured from 60 mm long borosilicate glass tubes. Care was taken to match their internal diameters to those of the test section in order to minimise any flow pattern disturbance. The thermal conductivity of the glass was estimated to be 1.14 W/mK, acting to reduce axial heat conduction. Flow patterns were recorded at the inlet sight glass by a specialised Photron Mini-UX high-speed camera, with a maximum resolution of 1 280 by 1 024 pixels, a maximum frame rate of 4 000 frames per second, and an internal recording capacity of 8 gigabytes. It was operated at 1 000 frames per second at a resolution of 1 280 × 720 pixels viewing the flow from the side. These settings enabled six seconds of recording time. Backlighting was provided by a red light-emitting diode measuring 50 mm by 50 mm.

Pressure transducers were attached to pressure taps, which were machined as described previously, and were 0.8 m (L_h) apart. Additionally, a Validyne differential pressure transducer, with an accuracy of 0.5% of the full scale, was also mounted to these pressure taps.

The test section thermocouple stations are indicated by the symbol **T** in Fig. 3. These stations each consisted of four T-type thermocouples, spaced equally around the circumference of the tube (right, top, left and bottom). The inlet and outlet saturation temperatures were measured by a thermocouple station before the inlet sight glass, and a thermocouple station after the outlet sight glass. These thermocouples were specifically placed to take advantage of the heat insulation provided by the high axial heat resistance of the sight glass. The obtained saturation temperature was cross-checked with the high-accuracy Pt100 RTDs that were installed in the flow passage directly before and after the test section. The saturation temperature was also compared to the expected saturation temperature at the operating pressure of the test section, obtained using reference libraries. A photograph of the inlet sight glass is shown in Fig. 4 before installation, detailing thermocouple station $\mathbf{T_{in}}$.

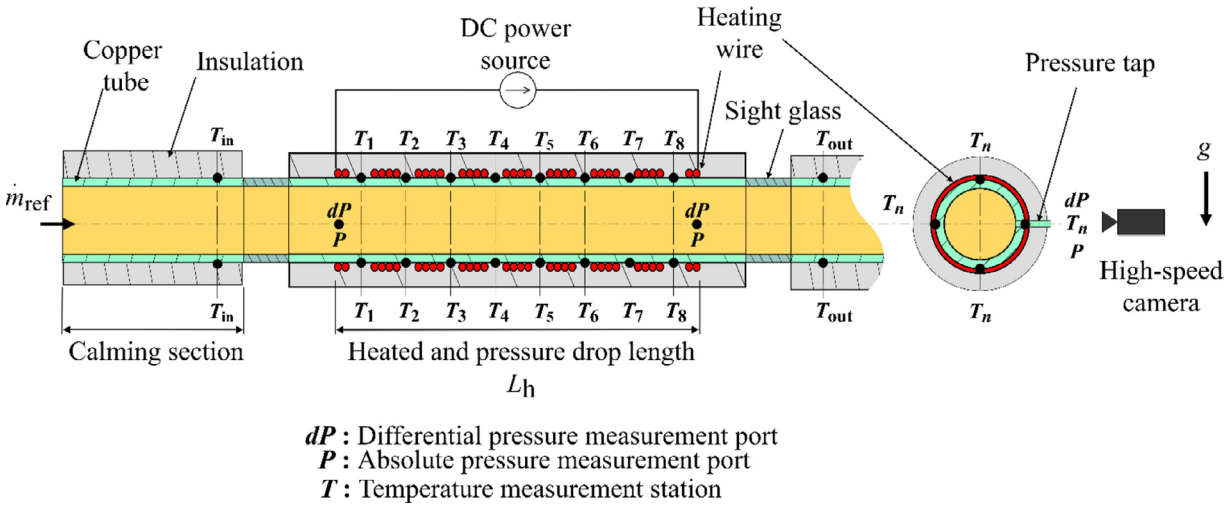


Fig. 3. Test section schematic (not to scale).

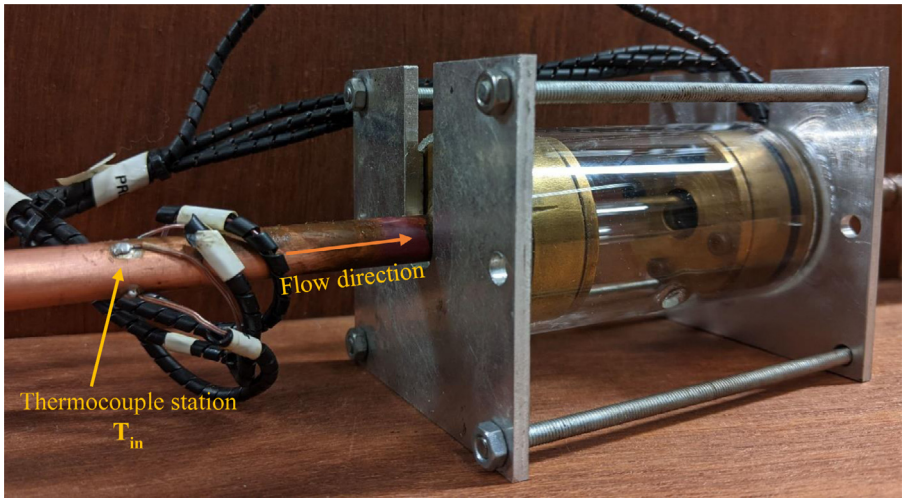


Fig. 4. Inlet sight glass before installation.

In addition, a further eight thermocouple stations were used to obtain the wall temperature in the heated length. The stations on the heated length were axially located 0.1 m apart. Therefore, in total, 32 thermocouples (eight stations) on the heated length and eight thermocouples (two stations) on the unheated length were used. They were all recessed within drilled divots in the tube wall and soldered, with special care being taken in the spacing between the heating wire and the thermocouples on the heated length to prevent localised overheating.

A photograph indicating the inlet pressure tap, the thermocouple station $\mathbf{T_1}$, and the heating wire is shown in Fig. 5 for clarity. This image was taken before insulation was added and the sight glass connected. The spacing and installation method for the thermocouples followed the empirical work by Everts [29], with the high thermal conductivity of copper compensating for the gap.

The same type of insulation that was used on the facility was applied to the test section, to a minimum radius of 0.1 m.

2.3. System control and data logging

A National Instruments data acquisition system (DAQ) was used in conjunction with a PC and a National Instruments LabView frontend for control of the system and data logging. The sample rate was chosen to be 300 Hz, and the number of samples per channel was set to 100. The virtual instrumentation used to control the power supply units, described below, limited the data output rate to approximately 2 Hz. The acquisition and control cards, which are described below, were mounted in a SCXI-1001 chassis.

The mass flow rate of the refrigerant fluid was controlled by the gear pump speed, which could be selected by adjusting the GATHER frequency control setting with a manual interface, or via LabView with an NI SCXI-1325 control card. As mentioned previously, the bypass valve could be adjusted manually to achieve fine flow control. The mass flow rate of the water in the condenser was controlled using a Honeywell three-way valve and an NI SCXI-1325 control card. This valve was powered by a separate AC power supply.

The Coriolis mass flow meters described previously sent the flow rate data of both the refrigerant fluid and the condenser loop water to LabView via an NI SCXI-1308 acquisition card.

The power supplies were connected to the computer with a USB cable from built-in control cards, and were controlled with either a LabView interface, or manually, bypassing the need for a chassis control card.

The thermocouples were connected to an NI SCXI-1303 acquisition card, from which the data was sent directly to LabView. Similarly, the Pt100 RTDs were connected to an NI SCXI-1306 card. The absolute pressure readings were obtained by connecting the pres-

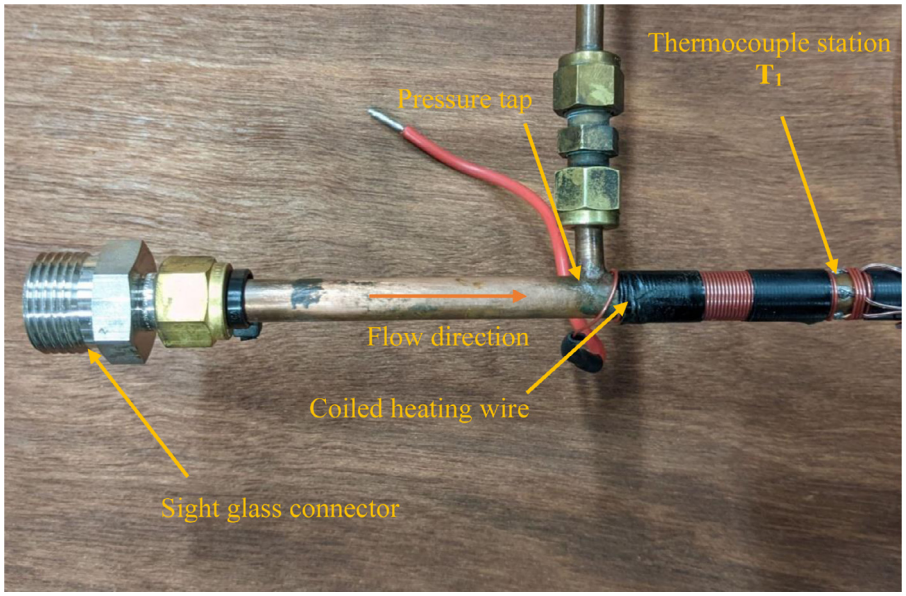


Fig. 5. Photograph detailing the uninsulated heated length inlet.

sure transducers, powered by a separate DC power supply, to an NI SCXI-1308 card, which was also used to connect the differential pressure transducer.

3. Experimental procedure

3.1. Calibration

Before installing the Pt100 RTDs and the thermocouples, shown in Fig. 2, they were calibrated in a thermal bath during a series of isothermal experiments by making use of a factory-calibrated Pt100 with an accuracy of 0.03 °C.

The thermocouples that were soldered onto the test section, and which are indicated in Fig. 3, were calibrated *in situ* once the system was charged with refrigerant. This was done by utilising the calibrated Pt100s mounted ahead and after the test section while circulating a single-phase fluid through the system. A calibration temperature reading was taken only if the two Pt100s read within 0.03 °C of each other for at least 10 min. This was repeated for a range of set temperatures.

The calibration of the absolute pressure transducers was done by an external calibration company, confirming an accuracy of less than 0.2%. A water column was used to provide differential pressures to a Martel T140 digital manometer, with an accuracy of 0.05% of full scale. These readings were then used to calibrate the differential pressure transducer.

3.2. Test matrix

The set points are shown in Fig. 6a on the Wojtan-Ursenbacher-Thome [30] flow pattern map. The map was adapted specifically for the current study, following the guidelines in Ref. [30]. The test matrix covered mass fluxes of 40, 60 and 80 kg/m^2 s at heat fluxes of 2.5, 5.0 and 7.5 kW/m^2 over an inlet vapour quality range from 0.05 until dryout occurred (which depended on the mass flux and heat flux in question). The governing flow patterns of interest to this study according to the map are: stratified flow, slug and stratified flow, and stratified wavy flow. The example flow patterns in Fig. 6b were obtained from the recorded high-speed camera footage. The heat flux in the test section raised the vapour quality, and this change depended on both the mass and heat flux. The lowest difference between inlet and outlet vapour quality occurred at a mass flux of 80 kg/m^2 s and a heat flux of 2.5 kW/m^2, and was 0.06. The highest value of this difference was at a mass flux of 40 kg/m^2 s and heat flux of 7.5 kW/m^2 and had a value of 0.35.

Since there was no heat exchange between Points B and C in Fig. 2, and the system was well insulated, an adiabatic condition was assumed to exist between the exit of the preheater and the test section inlet. With the addition of the calming section, as detailed previously, it was assumed that the flow patterns reaching the test section inlet were largely undisturbed.

3.3. Data processing

The preheater was used to ensure that the fluid was always in the saturation region at a selected vapour quality at the inlet to the test section. This was confirmed visually by means of the inlet sight glass, and experimentally by confirming that the saturation temperature stayed constant throughout the heated length of the test section. Only once this was verified did the tracking of steady state commence.

Steady-state conditions were carefully checked by monitoring the mass flux, the calculated inlet vapour quality and the saturation temperature. Data recording was initiated only when the variations in mass flux were less than 5%, the vapour quality variations were less than 0.01 (1%), and the saturation temperature was stable within 0.5 °C for a period of 15 min. Once these conditions were met, data was recorded for 5 min. The 8 stations of 4 thermocouples each (thus 32 thermocouples) along the length of the test section were each sampled approximately 600 times per 5 minute recording. The temporal mean of the readings was used in the data processing described in this section.

A heat loss calculation was performed to gauge the effect the ambient laboratory conditions would have on the test data. A thermal resistance network was constructed in which the conductive thermal resistance of the insulation, the convective thermal resistance of the laboratory, and the radiative thermal resistance were considered. Calculations showed that the effect on the heat in the test section was less than 1% at the worst case, and thus was disregarded in the rest of the data processing.

The local heat transfer coefficient along the length of the test section for each temperature measurement station (α_n) was deter-

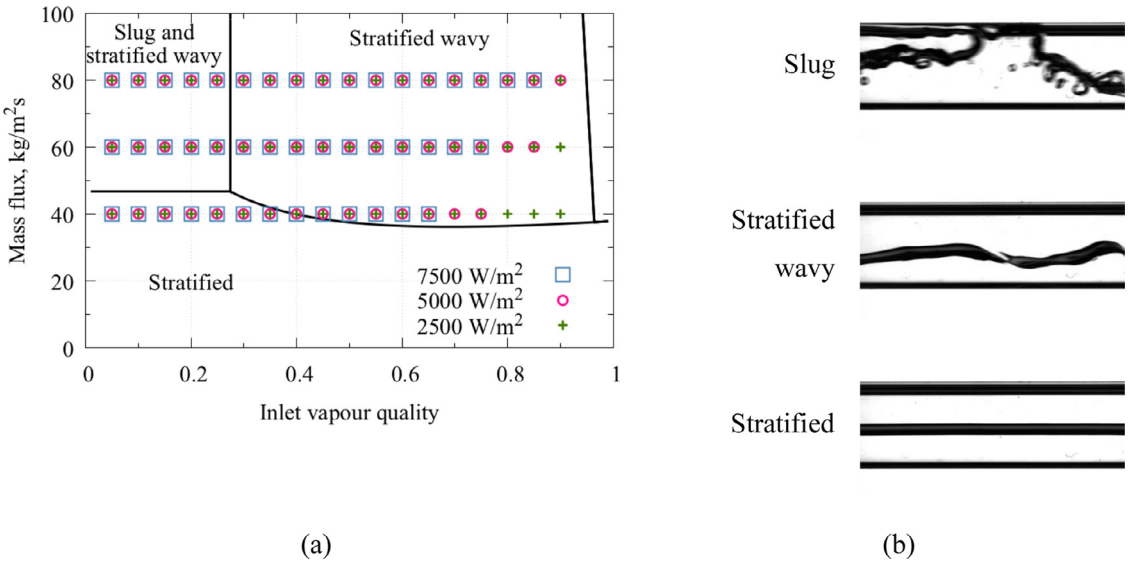


Fig. 6. (a) Test section inlet vapour qualities on a Wojtan-Ursenbacher-Thome [30] flow pattern map, along with (b) representative flow pattern images captured from the experimental facility.

mined using Newton's law of cooling:

$$\alpha_n = \frac{\dot{q}_{test}}{\left(\bar{T}_{i,n} - T_{sat}\right)} \tag{1}$$

Here, n represents the thermocouple station index number and $\dot{q}_{test}$ is the local uniform heat flux calculated from the total applied heat rate ($\dot{Q}_{test}$) and the total heated length inner surface area ($A_s = \pi d_i L_h$):

$$\dot{q}_{test} = \frac{\dot{Q}_{test}}{A_s} \tag{2}$$

In Eq. 1, $\bar{T}_{i,n}$ is the circumferential mean inner-wall temperature determined from the arithmetic average of the four wall thermocouples at the measuring station. A simple Fourier one-dimensional conduction equation was used to account for radial temperature variation within the wall. The average saturation temperature of the fluid, T_{sat}, was taken as the mean of the two measuring stations before and after the heated length (which resulted in an average of eight thermocouples). The inevitable drop in saturation temperature due to the pressure drop was thus accounted for. This was verified by comparing the measured saturation pressure with the calculated saturation pressure, using the reference software package CoolProp [31], based on the measured saturation temperature. In general, this difference was below 5 kPa, within the absolute pressure transducer's accuracy.

The total heat rate applied was taken to be the total power supplied by the power supply, which is given by the generalised power equation:

$$\dot{Q}_{test} = VI \tag{3}$$

where the voltage and current supplied are denoted by $V$and I respectively. Energy losses were estimated with convection, conduction and radiation losses to the ambient to be less than 0.1%, and were neglected.

The fluid entered the test section at a set mass flow rate ($\dot{m}_{ref}$), according to the operation of the variable-speed gear pump and bypass line valve. As such, the vapour quality at the inlet to the test section (x_{in}) was regulated by changing the heat transfer rate in the preheater. This vapour quality was defined as:

$$x_{in} = \frac{h_{in} - h_f}{h_g - h_f} \tag{4}$$

where the saturated liquid and vapour specific enthalpy values (h_f and h_g respectively) were calculated with CoolProp [31] at the measured saturation temperature T_{sat}. The specific enthalpy at the test section inlet, h_{in}, was obtained by using the energy balance between Points A (preheater inlet) and C (test section inlet) indicated in Fig. 2. For adiabatic conditions on the connecting flow tubes between the preheated and the test section, this energy balance can be expressed as:

$$h_{in} = h_C = h_B = \frac{\dot{Q}_{pre}}{\dot{m}_{ref}} + h_A \tag{5}$$

where $\dot{Q}_{pre}$ is the heat transfer rate in the preheater determined in the same fashion as in Eq. 2 using the voltage and current measurements at the preheater, h_A is the subcooled liquid specific enthalpy of the refrigerant at Point A, determined via CoolProp [31] using the absolute pressure and temperature readings ahead of the preheater. The mass flow rate was directly obtained from the refrigerant mass flow meter.

The applied heat flux was circumferentially uniform because of the heating wire being coiled around the pipe, and axially uniform at the inner surface because of the high thermal conductivity of copper. The local vapour qualities at each temperature station along the heated length could thus be calculated by linear interpolation between the inlet vapour quality, x_{in}, and vapour quality at the outlet of the heated section, x_{out}. In order to calculate x_{out}, the outlet enthalpy first had to be calculated:

$$h_{out} = \frac{\dot{Q}_{test}}{\dot{m}_{ref}} + h_{in} \tag{6}$$

From this the outlet quality could be determined:

$$x_{out} = \frac{h_{out} - h_f}{h_g - h_f} \tag{7}$$

Due to the low mass fluxes that were investigated, the condenser was oversized to a large degree, making an energy balance incorporating the heat removed by the condenser difficult. Nevertheless, this was still useful as a means to confirm steady state, and to ensure that no dominant source of energy loss had been left unaccounted. The energy balance error is given by:

$$\%EB = 100\left(1 - \frac{\dot{Q}_{pre} + \dot{Q}_{test}}{\dot{Q}_{cond}}\right) \tag{8}$$

Table 2
Parameter ranges and uncertainties.

Parameter	Range	Uncertainty
Singular temperature measurement point	17.5–40 °C	0.1 °C
Mass flux (G)	40–80 kg/m^2 s	0.6%
Inlet vapour quality (x_{in})	0.05–0.95	0.04
Heat flux ($\dot{q}$)	2.5–7.5 kW/m^2	0.4%
Heat transfer coefficient (α)	0.55–2.0 kW/m^{2}K	4%

where $\dot{Q}_{cond}$ is the heat transfer rate in the condenser, which was calculated by applying the energy balance principle and the water-side measurement:

$$\dot{Q}_{cond} = \dot{m}_w c_p (T_{w,out} - T_{w,in}) \quad (9)$$

Here, $\dot{m}_w$ is the water mass flow rate obtained from the water flow meter, $T_{w,\,out}$ is the temperature of water leaving the condenser, $T_{w,in}$ is the temperature of water entering the condenser, and c_p the isobaric specific heat capacity of water. The water temperatures were obtained from the relevant thermocouples and CoolProp was used to determine the specific heat capacity with the temperature measurements and the assumption that the water pressure was at approximately the atmospheric pressure of 82 kPa.

Finally, in order to account for the response time of the copper pipe in the test section, the Biot number was calculated, which is defined as:

$$Bi = \frac{\alpha L_c}{k} \quad (10)$$

where α represents a steady-state heat transfer coefficient, k is the thermal conductivity of copper, and L_c is the characteristic length of the test pipe, defined as:

$$L_c = \frac{V_{Cu}}{A_s} = \frac{\frac{\pi}{4}\left(d_o^2 - d_i^2\right)L_h}{\pi d_i L_h} = \frac{d_o^2 - d_i^2}{4d_i} \quad (11)$$

where V_{Cu} is the volume of the copper pipe. This was calculated throughout the tests performed and was always an order of magnitude below 0.1, which is the generally accepted limit when regarding temperature as uniform throughout a substance.

3.4. Uncertainty analysis

The uncertainties of the calculated variables and collected data were determined using the method by Dunn and Davis [32]. The range of values and uncertainties associated with these ranges are reported in Table 2.

3.5. Validation

In order to verify that the facility was performing correctly, a single-phase liquid validation as well as a two-phase boiling validation was done. The single-phase liquid validation consisted of obtaining experimental Nusselt numbers at various Reynolds numbers, ensuring that the measured wall temperature stayed well below the saturation temperature to avoid subcooled boiling. These results were then compared to some predicted values by the Gnielinski [33] and the recently much improved and accurate Meyer *et al.* correlation [34]. The obtained results are shown in Fig. 7a, and fell well within the 10% prediction window. Fig. 7b contains the energy balance in the test section for the tests, which was satisfactory.

Also important in giving confidence in the quality and reliability of the generated data were a series of two-phase boiling validation tests. This validation exercise was done at higher mass fluxes than would be considered for this work, and was done in order to confirm the results that would be obtained during this study. A steady-state test, with a mass flux of 200 kg/m^2 s and heat flux of 7.5 kW/m^2, at a saturation temperature of 35 °C, was done over the full range of vapour qualities. The resulting heat transfer coefficient is shown in Fig. 8. Since no results found in the literature replicate the current study exactly for comparison, it was decided to use some well-known correlations to predict the heat transfer coefficient. The experimental values obtained were then compared and checked against other published works in order to ascertain whether the results were acceptable. The predicted Wojtan-Ursenbacher-Thome [35], Fang et al. [36] and Gungor-Winterton [37] correlation values are also shown in the figure.

The experimental heat transfer coefficient was within ±10% of that predicted by the Wojtan-Ursenbacher-Thome [35] correlation, except at the extreme values of vapour quality. It also fell well within this range for predictions by the Fang et al. [36] correlation, and within ±30% for predictions by the Gungor-Winterton [37] correlation. This was comparable with most other published works for the mass flux, heat flux and tube diameter considered. Therefore, it can be deduced that the facility and test section produced satisfactory results in accordance with reported work in the literature.

4. Results and discussion

The local heat transfer coefficients obtained from the eight measuring stations along the test section length are shown in Fig. 9 in terms of the local vapour quality. Each combination of heat flux and mass flux in the test matrix is contained in individual plots (Fig. 9a to i). For convenience, the associated set of local heat transfer coefficients along the length of the test section obtained for each inlet vapour quality condition (see Fig. 6a) are grouped by feint lines. Due to the spread in the data, these groupings are most visible in Figs. 9a, d and g. Thus, the data for a single test case with a specified inlet vapour quality test is represented by eight data point markers (one per thermocouple station) connected by a feint line. The blue to red shaded lines represent a general increase in the inlet vapour quality cases in each data set (blue indicating the lower inlet vapour qualities and red indicating the higher inlet vapour qualities). For clarity, Fig. 9a contains a dashed line box around a single test case for an inlet vapour quality of 0.05, indicating the inlet thermocouple by the number one, and the outlet thermocouple by the number eight. Also included for illustrative purposes in Fig. 9 are the error bars. When compared to the calculated uncertainty in Table 2, it is clear that the variations along the axis of the pipe far exceed the uncertainty value. In each figure (Fig. 9a to i), the included black lines indicate the overall arithmetic mean of the heat transfer coefficient in the test section.

It can be seen that for the heat fluxes of 5.0 and 7.5 kW/m^2, for all the mass fluxes considered, all eight local heat transfer coefficients are much the same, such that the average heat transfer coefficient is a reasonable approximation. However, this approximation is not acceptable for the heat flux of 2.5 kW/m^2. The heat transfer coefficient in the first half of the tube is significantly higher. Because these high heat transfer coefficients were observed for all three mass fluxes, with separate mass fluxes being tested on different days, this was deemed significant.

4.1. Effect of mass flux on the heat transfer coefficient

The effect of mass flux on the heat transfer coefficient is illustrated in Fig. 10, in which the mean heat transfer coefficient profile for different mass fluxes is plotted against the mean test section vapour quality and the mass flux at heat fluxes of 2.5 kW/m^2

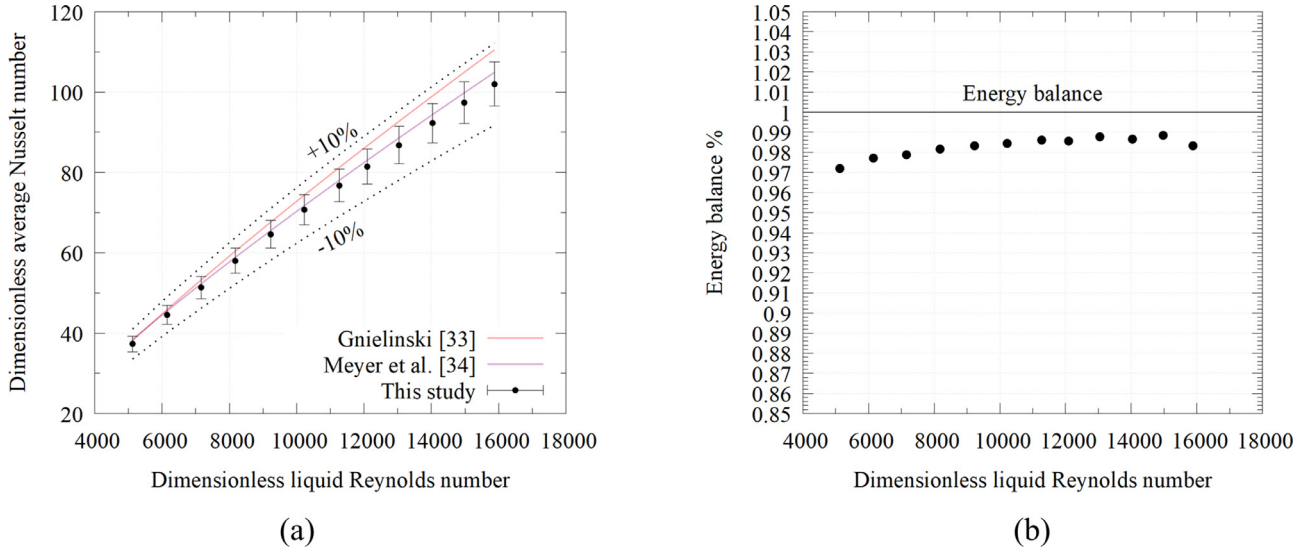


Fig. 7. Single-phase validation: (a) Nusselt number as a function of Reynolds number and (b) the energy balance over the test section at fluid inlet temperature 25°C.

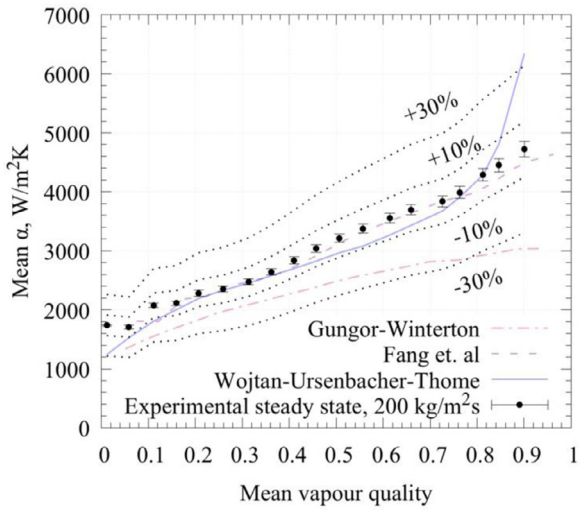


Fig. 8. Two-phase flow validation, showing steady-state mean heat transfer coefficient for a mass flux of 200 kg/m^{2}s, a heat flux of 7.5 kW/m^2 and a saturation temperature of 35 °C with predicted values.

(Fig. 10a), 5.0 kW/m^2 (Fig. 10b) and 7.5 kW/m^2 (Fig. 10c). The vapour quality is again indicated as a palette colour, in which blue is a quality of 0 and red a quality of 1.0. To show that these charts depict the same data, but from a different perspective, a point of interest (P.O.I.) is highlighted in Fig. 10a. This point was chosen to illustrate the peak in heat transfer coefficient at a mean vapour quality of approximately 0.25.

For the 2.5 kW/m^2 cases in Fig. 10a, it is clear that the mass flux has a marked influence on the magnitude of the average heat transfer coefficient, with the 80 kg/m^{2}s line always being above the 60 kg/m^{2}s line, which is, in turn, always above the 40 kg/m^{2}s line. A local maximum at a vapour quality of approximately 0.25 (designated P.O.I.) occurs. Here, there is an almost 150% increase in the heat transfer coefficient between mass fluxes 40 and 80 kg/m^{2}s. Increasing the vapour quality beyond this causes it to decrease sharply, up to a threshold value of 0.40. Beyond this threshold, a mass flux of 80 kg/m^2 s shows a steady increase in heat transfer coefficient as the vapour quality increases, while this effect is subdued at mass fluxes of 40 and 60 kg/m^{2}s. The second peak difference in heat transfer coefficient between mass fluxes of 40 and 80 kg/m^{2}s happens at a vapour quality of approximately 0.80. Here, the higher mass flux shows a 125% increase in heat transfer coefficient.

When considering 5.0 kW/m^2 cases in Fig. 10b, the mass flux also affects the heat transfer coefficient, but to a lesser extent. The initial local maximum is absent, while the effect of the increasing heat transfer coefficient beyond a threshold in vapour quality of 0.40 is still there for a mass flux of 80 kg/m^{2}s, but it is lower than for a heat flux of 2.5 kW/m^2. The peak difference between 40 and 80 kg/m^{2}s of 100% again occurs at an approximate vapour quality 0.85. For mass fluxes of 40 and 60 kg/m^{2}s, increasing the vapour quality actually slightly reduces the heat transfer coefficient. Nucleate boiling is dominant for these mass fluxes, which explains why there is no increase in heat transfer coefficient as the vapour quality increases. The flow patterns for these mass fluxes are predominantly stratified. Reasons for the decrease are discussed in depth in the flow pattern section (Section 4.3).

Finally, for the tests with 7.5 kW/m^2, shown in Fig. 10c, the behaviour mirrors that of the two other heat fluxes in that the higher mass flux always has a higher heat transfer coefficient. The initial peak for the heat flux of 2.5 kW/m^2 is absent, and the increase in heat transfer coefficient beyond a vapour quality of 0.40 for a mass flux of 80 kg/m^{2}s is subdued. The peak difference between 40 and 80 kg/m^{2}s occurs at a vapour quality of approximately 0.85, and is only 70% for this case.

The suggested cause of the behaviour of the heat transfer coefficient and the peaks at lower heat fluxes is also discussed in the flow pattern section (Section 4.3).

4.2. Effect of heat flux on the heat transfer coefficient

The mean heat transfer coefficient profile for different heat fluxes is plotted against the mean test section vapour quality at mass fluxes of 40 kg/m^{2}s (Fig. 11a), 60 kg/m^{2}s (Fig. 11b) and 80 kg/m^{2}s (Fig. 11c) in order to illustrate the effect of the heat flux on the heat transfer coefficient. Again, the vapour quality is indicated as a palette of colours on both charts. The same P.O.I. that is shown in Fig. 10a, at the highest heat transfer coefficient, is indicated in Fig. 11c.

Consider Fig. 11a for a mass flux of 40 kg/m^{2}s. For all data points for this mass flux, except for the results at the vapour qualities less than 0.40 at a heat flux of 2.5 kW/m^2, it is clear that

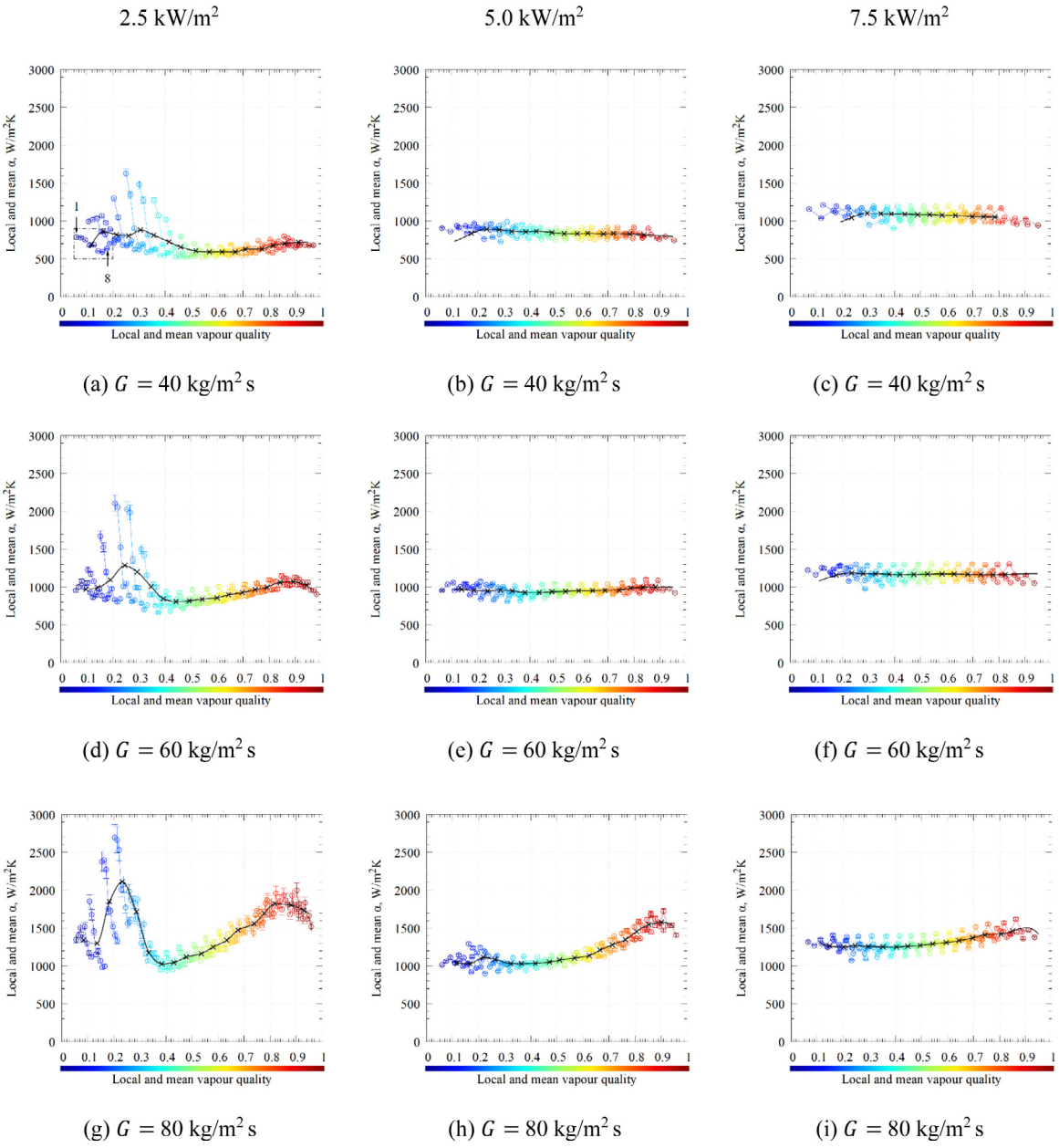


Fig. 9. Local heat transfer coefficient plotted against local vapour quality for a mass flux of: (a-c) 40 kg/m^2 s, (d-f), 60 kg/m^{2}s, and (g-i) and 80 kg/m^{2}s, at a saturation temperature of 35 °C.

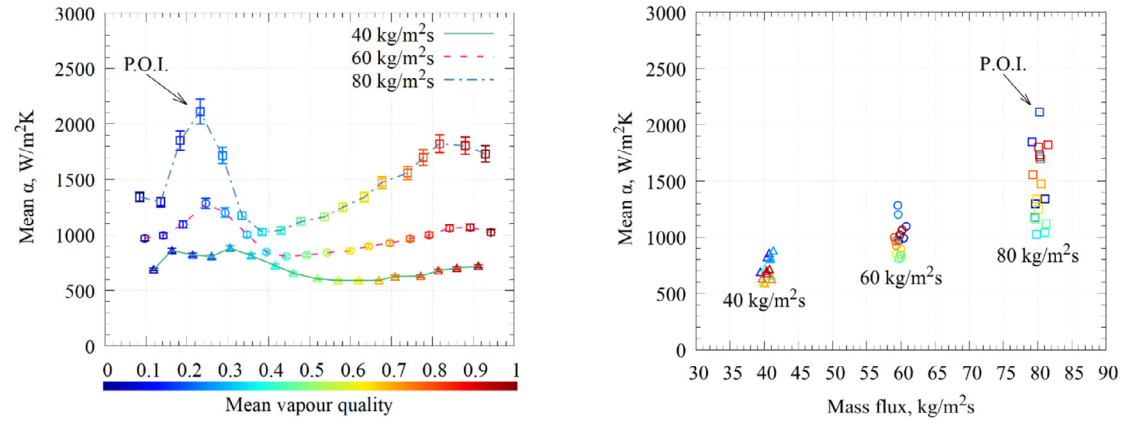
the higher heat flux results in an increased heat transfer coefficient. This effect does not happen only at low vapour qualities, as reported by other authors, but throughout the quality range. Fig. 11b indicates that for a mass flux of 60 kg/m^{2}s, again disregarding the heat flux of 2.5 kW/m^2, the heat transfer coefficient is higher for the higher heat flux throughout the quality range. In Fig. 11c, for a mass flux of 80 kg/m^{2}s, another oddity can be observed at vapour qualities in the region of 0.7 to 0.9 where another peak in the heat transfer coefficient is present. At a vapour quality exceeding approximately 0.40, the heat transfer coefficient increases with vapour quality, as reported, but for a heat flux of 2.5 and 5.0 kW/m^2 this effect is more pronounced.

4.3. Effect of flow pattern on the heat transfer coefficient

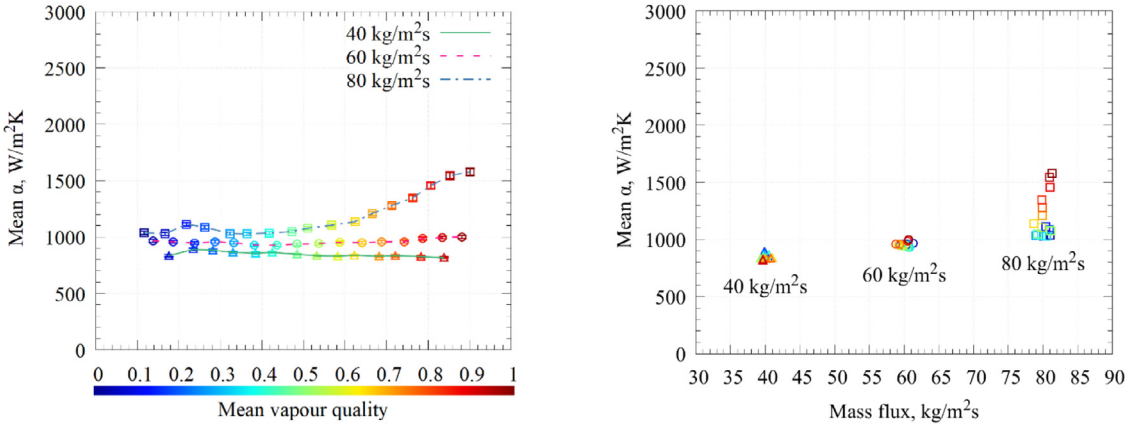
As discussed in the previous sections, at the lowest heat flux, low vapour qualities exhibit far larger heat transfer coefficients than expected for all mass fluxes. The heat transfer coefficient is up to 70% higher at the entry to the tube than the heat transfer coefficient at the exit of the tube for an inlet vapour quality of 0.20 and mass flux of 80 kg/m^2 s, as indicated in Fig. 12, which shows the local heat transfer coefficients zoomed for a single-inlet vapour quality test at the different thermocouple stations.

Additionally, the increasing vapour quality results in a higher heat transfer coefficient for a heat flux of 2.5, 5.0 and 7.5 kW/m^2 beyond a vapour quality of 0.40 for this mass flux, with the lower heat fluxes showing a larger effect, as shown in Fig. 11c.

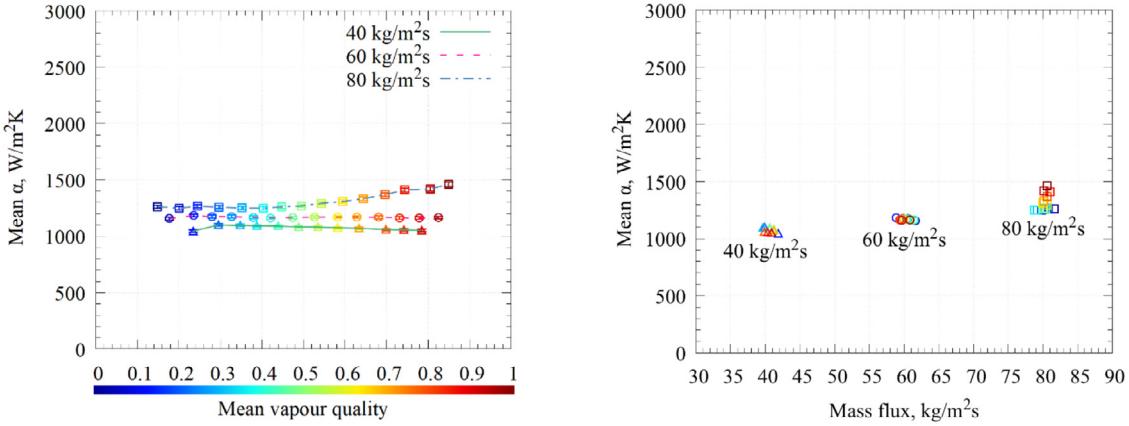
The peak in heat transfer coefficient at the inlet at a heat flux of 2.5 kW/m^2 is discussed first. Initially, it was thought that steady state had not been achieved for these specific qualities, but that idea was discarded immediately, since after cursory investigation, the temperatures at all thermocouple stations were stable for the 5 min required to record a set of data. The possibility of user error



(a) 2.5 kW/m^2

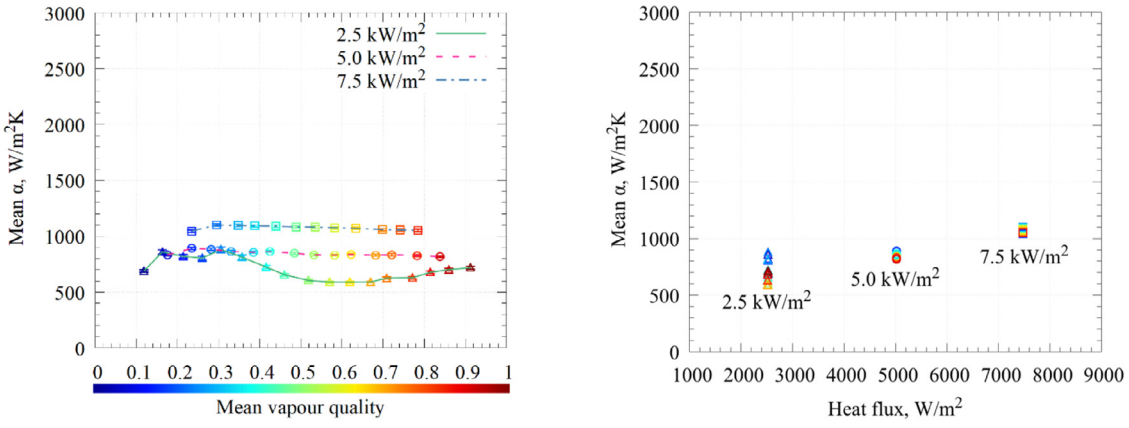


(b) 5.0 kW/m^2

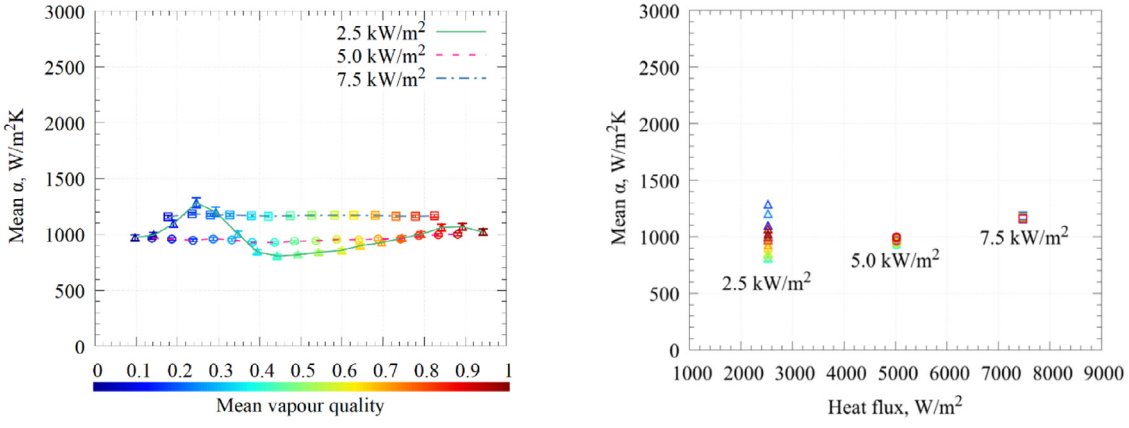


(c) 7.5 kW/m^2

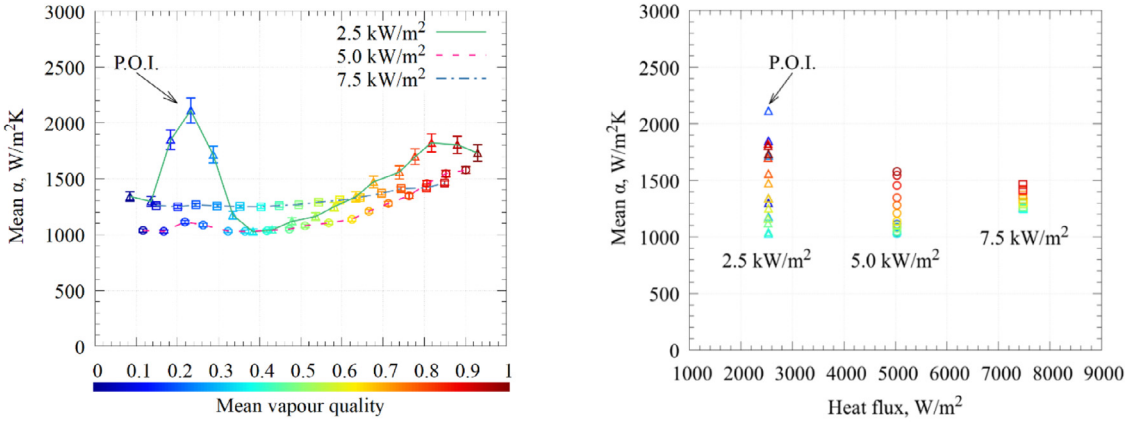
Fig. 10. Effect of mass flux on the mean heat transfer coefficient for heat fluxes of: (a) 2.5 kW/m^2, (b) 5.0 kW/m^2 and (c) 7.5 kW/m^2.



(a) 40 kg/m² s



(b) 60 kg/m² s



(c) 80 kg/m² s

Fig. 11. Effect of heat flux on the mean heat transfer coefficient for mass fluxes of: (a) 40 kg/m² s, (b) 60 kg/m² s, and (c) 80 kg/m² s.

in setting up the experiment was also discarded, because the data was gathered over different days for the different conditions.

The possibility that the flow patterns differed between heat fluxes at the inlet due to intrafluid axial heat conduction, accounting for the change in heat transfer coefficient, was investigated next. High-speed recordings of the vapour qualities at 0.15 to 0.35 were compared for a mass flux of 80 kg/m² s at a heat flux of 2.5 kW/m² and 5.0 kW/m². This mass flux was chosen because it showed the greatest discrepancy in heat transfer coefficient. It was found that the flow patterns for both heat fluxes were slug and

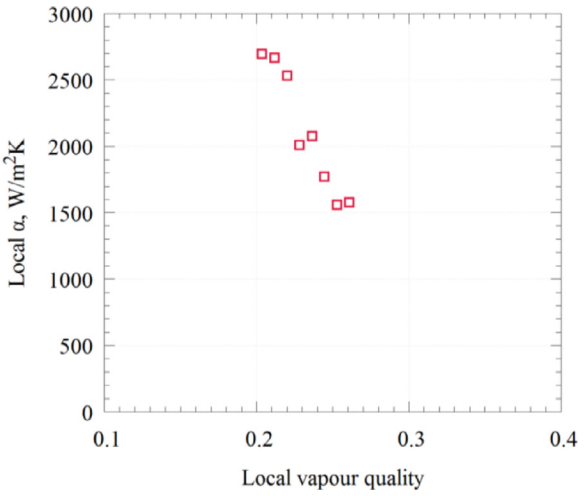


Fig. 12. Representative example at a mass flux of 80 kg/m^2 s and inlet vapour quality of 0.20 of the large difference between entry and exit heat transfer coefficients for a heat flux of 2.5 kW/m^2.

stratified wavy, with intermittent waves and slugs wetting the top of the tube. The flow patterns obtained for an inlet vapour quality of 0.20 are shown for illustrative purposes in Fig. 13.

Because the same behaviour was observed for the same mass flux at two differing heat fluxes, the idea that differing flow patterns were the cause of the discrepancy in heat transfer coefficient was discarded. However, it is the wetting of the top surface of the tube at this flow pattern that might hold the key to understanding the behaviour of the heat transfer coefficient.

In an adiabatic setting, the liquid fluid would prolong the wetting of the tube as it descended to the bottom of the tube naturally. It is hypothesised that at a high heat flux, this liquid film is boiled away quickly, leaving the top of the tube dry. At a lower heat flux, this film is boiled away more slowly, resulting in the high heat transfer coefficient observed at the inlet, decreasing with the spatial variation along the tube. This could also explain why the highest mass flux of 80 kg/m^2 s shows the most drastic increase in heat transfer coefficient, since the higher the mass flux is, the higher the frequency of intermittent wetting is. However, no direct link could be established between the frequency of this flow pattern variation and the wall temperature data, possibly due to a combination of the time constant of the thermocouples and the sampling rate that was used.

The flow patterns and heat flux can also be used to interpret the increase of the heat transfer coefficient beyond a vapour quality of 0.40 for a mass flux of 80 kg/m^{2}s while staying relatively constant for mass fluxes of 40 and 60 kg/m^{2}s (Fig. 10a) for a heat flux of 2.5 kW/m^2, or even decreasing for higher heat fluxes of 5.0 and 7.5 kW/m^2 (Figs. 10b and c). The flow patterns observed for the three mass fluxes in Fig 10a at a vapour quality of 0.40 and 0.70 are shown in Fig. 14 in order to explain this.

As can be seen in Figs.14a and 14b, the flow pattern transitions between a stratified wavy form at a vapour quality of 0.40 (where the wall is partially dry), to a hybrid annular/stratified wavy pattern (where the pipe wall is completely wet) at a vapour quality of 0.70, for a mass flux of 80 kg/m^2 s. This is contrasted with the pure stratified wavy flow pattern obtained for mass fluxes of 40 and 60 kg/m^2 s at all vapour qualities, in Fig. 14c to f.

For the hybrid/intermittent annular flow pattern, as the vapour quality increases, the liquid film wetting the top of the pipe becomes thinner, facilitating a higher heat transfer coefficient, as reported by other authors for mass fluxes higher than 80 kg/m^2 s. The almost negligible increase in heat transfer coefficient for mass fluxes of 40 and 60 kg/m^{2}s for a heat flux of 2.5 kW/m^2 results from a large portion of the pipe wall being dry throughout the vapour quality range.

At higher heat fluxes, the stratification (and thus the dry perimeter) is thought to be more pronounced at all mass fluxes. The mass fluxes of 40 and 60 kg/m^{2}s are insufficient to wet the pipe perimeter, resulting in a decreased heat transfer coefficient as the vapour quality increases and the dry portion of the perimeter becomes larger. The mass flux of 80 kg/m^{2}s shows an increase in heat transfer coefficient at the higher heat fluxes, although this increase is lower than at a heat flux of 2.5 kW/m^2. It is hypothesised that partial dryout of the top of the pipe wall at heat fluxes of 5.0 and 7.5 kW/m^2 may be the cause.

4.4. Comparison with correlations

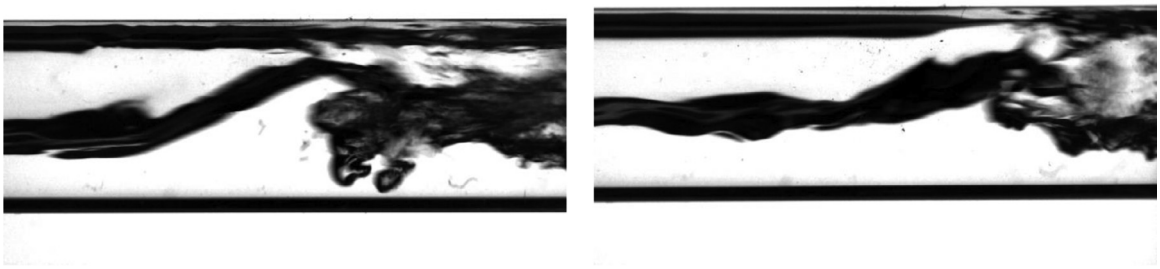
Some widely trusted correlations were used in an attempt to examine if any could capture the behaviour shown in Figs. 10a, 11c and 12. Specifically, the behaviour that needed to be replicated was the peak in heat transfer coefficient for lower vapour qualities in the first stages of the test section and the drastic reduction towards the exit of the tube.

Apart from the Fang et al. [36] correlation, all of these correlations incorporate the nucleate boiling contribution in some way. In the Liu-Winterton [38] and Gungor-Winterton [37] correlations, a boiling suppression factor is introduced, which is multiplied by the nucleate boiling contribution in the eventual summation to obtain the two-phase heat transfer coefficient. In the Bertsch et al. [39] correlation, the vapour quality for which the heat transfer coefficient is being predicted is combined with the nucleate boiling heat transfer coefficient before summation with the convective liquid and vapour heat transfer coefficients. The Kandlikar [40] correlation calculates the boiling heat transfer coefficient with a set of constants for the nucleate and convective boiling region separately, and chooses the maximum heat transfer coefficient, and the Wojtan-Ursenbacher-Thome [35] correlation implements a nucleate boiling contribution in the calculation of the wetted perimeter heat transfer coefficient. Moran et al. [26] investigated the applicability of pool boiling correlations to R-245fa boiling flows at nucleate boiling-dominant conditions but found them to have poor predictive capability for the experimental conditions.

The values of predicted heat transfer coefficient (pink empty circles) are compared with the actual heat transfer coefficient (blue filled circles), and are shown in Fig. 15 for different correlations and flows with a mass flux of 80 kg/m^2 s and heat flux of 2.5 kW/m^2.

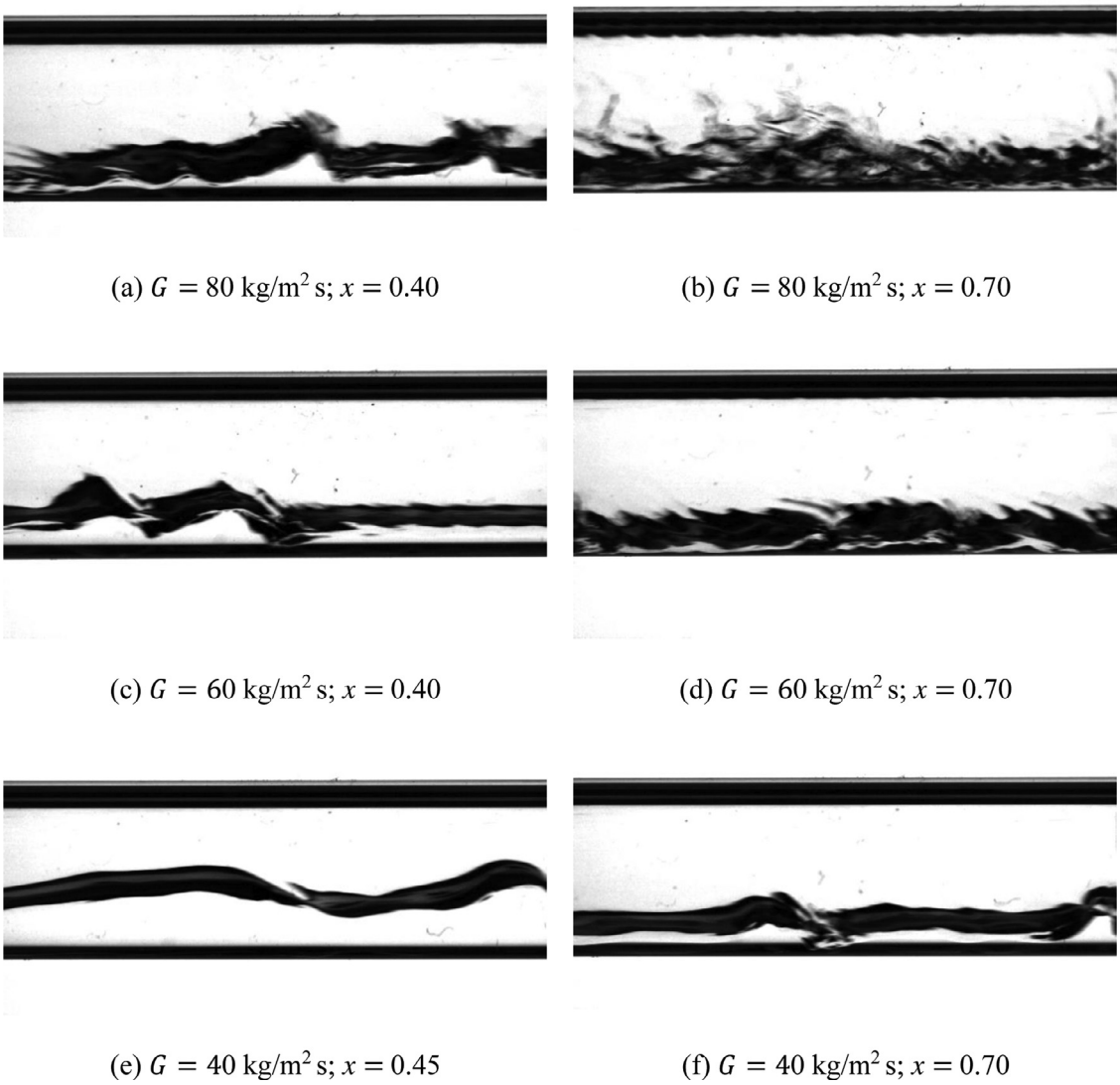
As can be seen in Figs. 15a to d, the correlations do not predict the peak at all, and only at higher qualities, where the flow pattern is assumed to be largely the same throughout the tube length, do the correlations of Liu-Winterton [38], Gungor-Winterton [37], and Kandlikar [40] start to predict within acceptable levels. The Fang et al. [36] correlation, shown in Fig. 15e, despite its apparent accuracy, is limited in application, because it uses the measured local wall temperature in its formulation. Therefore, the correlation cannot predict this local wall temperature iteratively. On the other hand, the flow pattern-based correlation of Wojan-Ursenbacher-Thome [35] captures the general trend of the heat transfer coefficient fairly well, although the accuracy is unsatisfactory.

Taking a step back to consider the correlations in Fig. 15a to f, and the data used to predict the heat transfer coefficient, it becomes clear that none of the correlation formulations have any way of accounting for changes between tube inlet and outlet. In hindsight, it seems obvious that some way of accounting for the changes happening in the tube needs to be applied. The Fang et al. [36] correlation takes this into account by using the actual wall temperature in the correlation. The flow pattern-based correla-



(a) 2.5 kW/m^2 (b) 5.0 kW/m^2

Fig. 13. Representative flow patterns at the inlet for a heat flux of: (a) 2.5 kW/m^2, and (b) 5.0 kW/m^2, at an inlet vapour quality of 0.20 and mass flux of 80 kg/m^2 s.



(a) $G = 80$ kg/m^2 s; $x = 0.40$ (b) $G = 80$ kg/m^2 s; $x = 0.70$

(c) $G = 60$ kg/m^2 s; $x = 0.40$ (d) $G = 60$ kg/m^2 s; $x = 0.70$

(e) $G = 40$ kg/m^2 s; $x = 0.45$ (f) $G = 40$ kg/m^2 s; $x = 0.70$

Fig. 14. Flow patterns illustrating the transition from stratified wavy flows to hybrid/intermittent flows for a mass flux of 80 kg/m^2 s and a heat flux of 2.5 kW/m^2.

tion of Wojtan-Ursenbacher-Thome [35] takes changes in the tube into account by predicting the flow pattern and adjusting the heat transfer correlation accordingly. Though the flow map is incorrect in exactly determining which flow pattern is present, and its accuracy is not sufficient for this case, it is felt that this approach is the only accurate way of calculating the heat transfer coefficient where the flow pattern changes inside a tube. Future studies will need to gather more data before attempting to adjust the correlation and the flow pattern map. Incorporating the known conditions and fluid properties into the flow pattern maps, and adjusting the hard cut-off lines for qualities and mass fluxes between flow patterns, seem to be the focus of future studies. Regardless, this study showed that flow pattern-based correlations are perhaps the only applicable means of predicting the heat transfer coefficient in

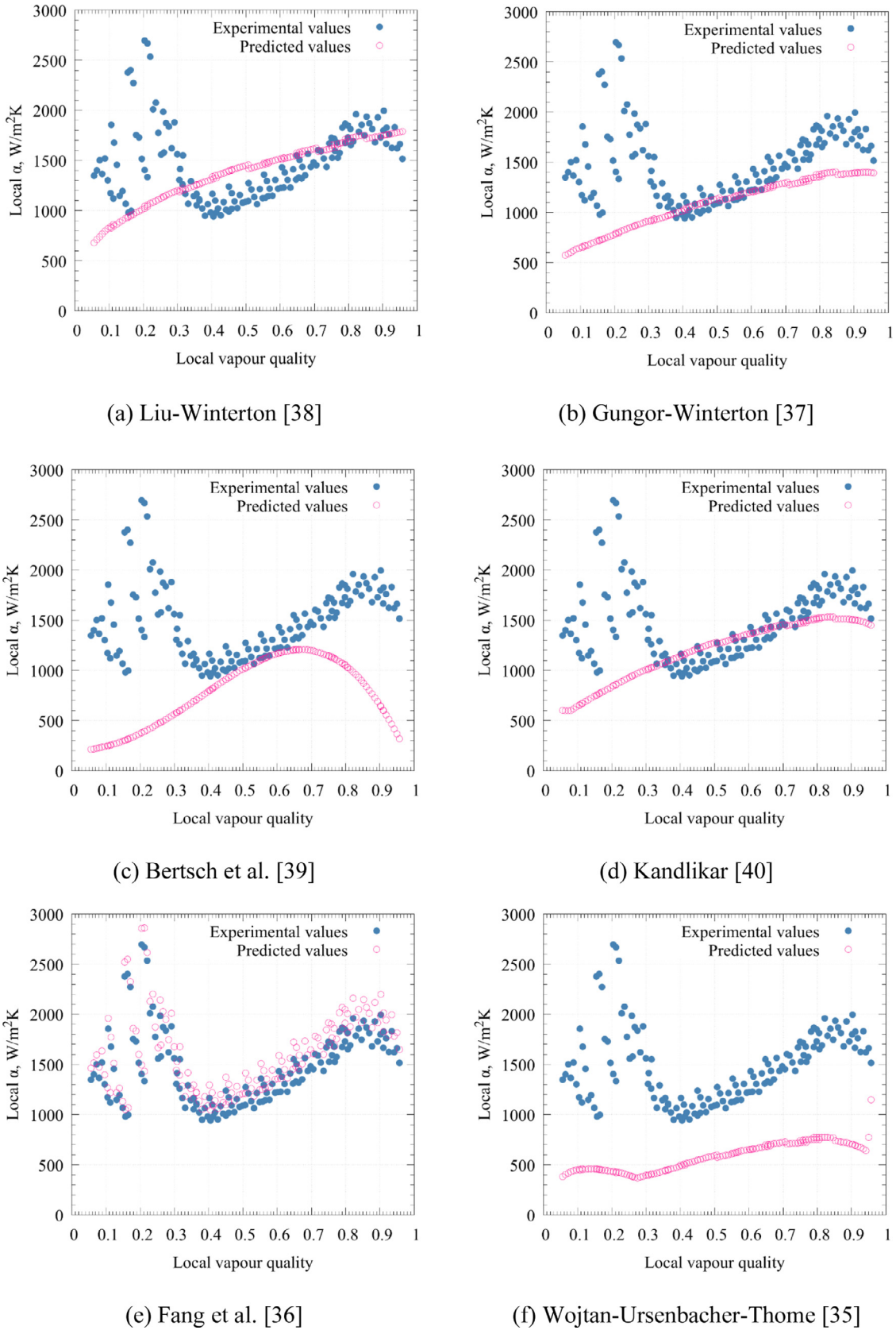


Fig. 15. Comparisons with heat transfer coefficient predictions from well-known correlations for a mass flux of 80 kg/m^2 s and a heat flux of 2.5 kW/m^2.

modern industrial applications where the mass and heat flux are relatively low.

5. Conclusions

Low mass and heat flux applications are becoming more prevalent, as are components and systems that rely on the boiling of refrigerants and specifically of R-245fa, making studies of the in-tube boiling behaviour of such refrigerants and at these conditions increasingly of interest. In particular, there is a growing need to find applicable correlations to predict the heat transfer coefficient in relevant flows. The following observations can be made for the in-tube flow boiling of R-245fa at low heat and mass fluxes, which was investigated experimentally in a dedicated facility in this work:

- The mass flux had an impact on the heat transfer coefficient, with an increasing mass flux resulting in a higher heat transfer coefficient, as found by most authors listed in Table 1.
- The results corresponding to flows with imposed mass flux values of 40 and 60 kg/m^2 s and heat flux values of 5.0 and 7.5 kW/m^2 showed the heat transfer coefficient was weakly dependent on the vapour quality. This is in agreement with findings from related research [23,24].
- However, for flows with a higher mass flux of 80 kg/m^2 s and for vapour qualities above 0.40, the heat transfer coefficient showed a definite increase with increasing vapour quality for all investigated heat fluxes. This was explained in terms of the flow pattern transitioning to a stratified wavy and annular hybrid/intermittent flow. It was also hypothesised that this was amplified at lower heat fluxes due to the properties of the fluid and the absence of dryout in the tube.
- For flows with the lowest imposed heat flux of 2.5 kW/m^2, peculiar behaviour was observed in the local heat transfer coefficients for vapour qualities between 0.15 and 0.35 at the inlet to the tube. When compared to extant values found in literature, those obtained for the two higher heat fluxes considered, and those predicted by common correlations, the heat transfer coefficients were abnormally high. This correlated with direct visual observations which confirmed the intermittent wetting of the tube wall by the combined slug and stratified wavy flow patterns. The conditions resulted in the tube wall staying wet for a larger portion of the test length.
- Well-known correlations were applied in an attempt to capture the peaks in heat transfer coefficient at a mass flux of 80 kg/m^2 s and a heat flux of 2.5 kW/m^2.
- The flow pattern-based method was the only correlation that could capture these peaks, although the accuracy was considered unsatisfactory for most design requirements.
- The flow pattern map was not sufficiently accurate to detect the flow pattern shift in the tube.
- Additional work needs to be done in order to improve the predictive power of such correlations which relies critically upon correctly capturing the flow patterns to account for these peaks.

It is recommended that more studies be conducted at low heat fluxes in order to verify the results of this study and to capture both the inlet and outlet flow pattern for comparison. A detailed frequency analysis at different sampling rates to gauge the effect of the flow pattern on the wall temperature should also be performed. The contribution of nucleate boiling in the correlations considered could also be investigated. Also of interest would be investigating the secondary flows induced in the fluid under non-uniform heat fluxes (as observed by Wang et al. [41] for mass fluxes of 193 to 386 kg/m^{2}s and heat fluxes of 10 to 36 kW/m^2) at the lower mass and heat fluxes in this study.

Declaration of Competing Interest

The authors declare that they have no known competing financial interests or personal relationships that could have appeared to influence the work reported in this paper.

CRediT authorship contribution statement

W.J. Van den Bergh: Conceptualization, Methodology, Validation, Data curation, Formal analysis, Writing – original draft. **H.R. Moran:** Formal analysis, Writing – review & editing. **J. Dirker:** Supervision, Funding acquisition, Formal analysis, Writing – review & editing. **C.N. Markides:** Supervision, Conceptualization, Funding acquisition, Writing – review & editing. **J.P. Meyer:** Supervision, Conceptualization, Funding acquisition, Writing – review & editing.

Acknowledgements

This work was supported by the Department for International Development (DFID) through the Royal Society-DFID Africa Capacity Building Initiative, and by the UK Engineering and Physical Sciences Research Council (EPSRC) [grant numbers EP/T03338X/1 and EP/P004709/1]. The work was also supported by Russian Government “Megagrant” project 075-15-2019-1888. Data supporting this publication can be obtained on request from ceplab@imperial.ac.uk.

References

[1] X. Fang, F. Zhuang, C. Chen, Q. Wu, Y. Chen, Y. Chen, Y. He, Saturated flow boiling heat transfer: review and assessment of prediction methods, Heat Mass Transf. 55 (1) (2019) 197–222.
[2] S.G. Kandlikar, W.J. Grande, Evolution of microchannel flow passages: thermohydraulic performance and fabrication technology, Heat Transf. Eng. 24 (1) (2003) 3–17.
[3] M.K. Smith, J.P. Wattelet, T.A. Newell, A study of evaporation heat transfer coefficient correlations at low heat and mass fluxes for pure refrigerants and refrigerant mixtures, 1993.
[4] R.L. Amalfi, F. Vakili-Farahani, J.R. Thome, Flow boiling and frictional pressure gradients in plate heat exchangers. Part 1: review and experimental database, Int. J. Refrig. 61 (2016) 166–184.
[5] C.N. Markides, Low-concentration solar-power systems based on organic Rankine cycles for distributed-scale applications: overview and further developments, Front. Energy Res. 3 (47) (2015).
[6] J. Dirker, D. Juggurnath, A. Kaya, E.A. Osowade, M. Simpson, S. Lecompte, S.M.A. Noori Rahim Abadi, V. Voulgaropoulos, A.O. Adelaja, M.Z. Dauhoo, A. Khoodaruth, S.O. Obayopo, O.T. Olakoyejo, M.K. Elahee, M. De Paepe, J.P. Meyer, C.N. Markides, Thermal energy processes in direct steam generation solar systems: boiling, condensation and energy storage – a review, Front. Energy Res. 6 (2019) 147.
[7] A.M. Pantaleo, S.M. Camporeale, A. Sorrentino, A. Miliozzi, N. Shah, C.N. Markides, Hybrid solar-biomass combined Brayton/organic Rankine-cycle plants integrated with thermal storage: techno-economic feasibility in selected Mediterranean areas, Renew. Energy 147 (2020) 2913–2931.
[8] J. Freeman, K. Hellgardt, C.N. Markides, Working fluid selection and electrical performance optimisation of a domestic solar-ORC combined heat and power system for year-round operation in the UK, Appl. Energy 186 (2017) 291–303.
[9] J. Freeman, K. Hellgardt, C.N. Markides, An assessment of solar-powered organic Rankine cycle systems for combined heating and power in UK domestic applications, Appl. Energy 138 (2015) 605–620.
[10] M. Gómez Marzoa, G. Ribatski, J.R. Thome, Experimental flow boiling heat transfer in a small polyimide channel, Appl. Therm. Eng. 103 (2016) 1324–1338.
[11] C.B. Tibiriçá, G. Ribatski, Flow Boiling heat transfer of R-134a and R-245fa in a 2.3 mm tube, Int. J. Heat Mass Transf. 53 (11) (2010) 2459–2468.
[12] F.T. Kanizawa, C.B. Tibiriçá, G. Ribatski, Heat transfer during convective boiling inside microchannels, Int. J. Heat Mass Transf. 93 (2016) 566–583.
[13] R.J. Da Silva Lima, J.M. Quibén, J.R. Thome, Flow boiling in horizontal smooth tubes: new heat transfer results for R-134a at three saturation temperatures, Appl. Therm. Eng. 29 (7) (2009) 1289–1298.
[14] C.A. Dorao, O.B. Fernandez, M. Fernandino, Experimental study of horizontal flow boiling heat transfer of R-134a at a saturation temperature of 18.6 °C, J. Heat Transf. (11) (2017) 139.
[15] A. Celen, A.S. Dalkılıç, A complete evaluation method for the experimental data of flow boiling in smooth tubes, Int. Commun. Heat Mass Transf. 89 (2017) 108–121.

[16] S. Grauso, R. Mastrullo, A. Mauro, J. Thome, G. Vanoli, Flow pattern map, heat transfer and pressure drops during evaporation of R-1234ze (E) and R-134a in a horizontal, circular smooth tube: experiments and assessment of predictive methods, Int. J. Refrig. 36 (2) (2013) 478–491.
[17] G. Bamorovat Abadi, C. Moon, K.C. Kim, Effect of gravity vector on flow boiling heat transfer, flow pattern map, and pressure drop of R-245fa refrigerant in mini tubes, Int. J. Multiphase Flow 83 (2016) 202–216.
[18] E.P. Bandarra Filho, P.E.L. Barbieri, Flow boiling performance in horizontal microfinned copper tubes with the same geometric characteristics, Exp. Therm. Fluid Sci. 35 (5) (2011) 832–840.
[19] E. Manavela Chiapero, M. Fernandino, C.A. Dorao, Experimental results on boiling heat transfer coefficient, frictional pressure drop and flow patterns for R-134a at a saturation temperature of 34°C, Int. J. Refrig. 40 (2014) 317–327.
[20] K. Spindler, H. Müller-Steinhagen, Flow boiling heat transfer of R-134a and R-404A in a microfin tube at low mass fluxes and low heat fluxes, in: Heat Mass Transf., 45, 2009, pp. 967–977.
[21] P. Balachander, B. Raja, Investigation on the boiling heat transfer characteristics of R-404A and R-134a under stratified flow condition, Heat Mass Transf. 51 (6) (2015) 825–835.
[22] E. Björk, B. Palm, Flow boiling heat transfer at low flux conditions in a domestic refrigerator evaporator, Int. J. Refrig. 31 (6) (2008) 1021–1032.
[23] J.M. Saiz Jabardo, E.P. Bandarra Filho, Convective boiling of halocarbon refrigerants flowing in a horizontal copper tube – an experimental study, Exp. Therm. Fluid Sci. 23 (3) (2000) 93–104.
[24] J.P. Wattelet, J.C. Chato, A.L. Souza, B.R. Christoffersen, Evaporative characteristics of R-134a, MP-39, and R-12 at low mass fluxes, ASHRAE Trans. 100 (1994) 603–615.
[25] J.P. Meyer, D.R.E. Ewim, Heat transfer coefficients during the condensation of low mass fluxes in smooth horizontal tubes, Int. J. Multiphase Flow 99 (2018) 485–499.
[26] H.R. Moran, D. Zogg, V. Voulgaropoulos, W.J. Van den Bergh, J. Dirker, J.P. Meyer, O.K. Matar, C.N. Markides, An experimental study of the thermo-hydraulic characteristics of flow boiling in horizontal pipes: linking spatiotemporally resolved and integral measurements, Appl. Therm. Eng. 194 (2021) 117085.
[27] J. Dirker, W.J. Van den Bergh, H.R. Moran, C.N. Markides, J.P. Meyer, Influence of inlet vapour quality perturbations on the transient response of flow-boiling heat transfer, Int. J. Heat Mass Transf. 170 (2021) 121017.
[28] K. Cho, S.-J. Tae, Condensation heat transfer for R-22 and R-407C refrigerant–oil mixtures in a microfin tube with a U-bend, Int. J. Heat Mass Transf. 44 (11) (2001) 2043–2051.
[29] M. Everts, Single-phase mixed convection of developing and fully developed flow in smooth horizontal tubes in the laminar, transitional, quasi-turbulent and turbulent flow regimes, University of Pretoria, 2017.
[30] L. Wojtan, T. Ursenbacher, J.R. Thome, Investigation of flow boiling in horizontal tubes: Part I—a new diabatic two-phase flow pattern map, Int. J. Heat Mass Transf. 48 (14) (2005) 2955–2969.
[31] I.H. Bell, J. Wronski, S. Quoilin, V. Lemort, Pure and pseudo-pure fluid thermophysical property evaluation and the open-source thermophysical property library CoolProp, Ind. Eng. Chem. Res. 53 (6) (2014) 2498–2508.
[32] Dunn, P.F. and Davis, M.P., *Measurement and data analysis for engineering and science*. 2018.
[33] V. Gnielinski, New equations for heat and mass transfer in turbulent pipe and channel flow, Int. Chem. Eng. 16 (2) (1976) 359–368.
[34] J.P. Meyer, M. Everts, N. Coetzee, K. Grote, M. Steyn, Heat transfer coefficients of laminar, transitional, quasi-turbulent and turbulent flow in circular tubes, Int. Commun. Heat Mass Transf. 105 (2019) 84–106.
[35] L. Wojtan, T. Ursenbacher, J.R. Thome, Investigation of flow boiling in horizontal tubes: Part II—development of a new heat transfer model for stratified-wavy, dryout and mist flow regimes, Int. J. Heat Mass Transf. 48 (14) (2005) 2970–2985.
[36] X. Fang, Q. Wu, Y. Yuan, A general correlation for saturated flow boiling heat transfer in channels of various sizes and flow directions, Int. J. Heat Mass Transf. 107 (2017) 972–981.
[37] K.E. Gungor, R.H.S. Winterton, A general correlation for flow boiling in tubes and annuli, Int. J. Heat Mass Transf. 29 (3) (1986) 351–358.
[38] Z. Liu, R.H.S. Winterton, A general correlation for saturated and subcooled flow boiling in tubes and annuli, based on a nucleate pool boiling equation, Int. J. Heat Mass Transf. 34 (11) (1991) 2759–2766.
[39] S.S. Bertsch, E.A. Groll, S.V. Garimella, Refrigerant flow boiling heat transfer in parallel microchannels as a function of local vapor quality, Int. J. Heat Mass Transf. 51 (19) (2008) 4775–4787.
[40] S.G. Kandlikar, A general correlation for saturated two-phase flow boiling heat transfer inside horizontal and vertical tubes, J. Heat Transf. 112 (1) (1990) 219–228.
[41] D. Wang, L. Zhao, X. Nie, Y. Lu, S. Deng, Experimental study on flow boiling characteristics of R-245fa in circular tube under non-uniform heat flux, Int. J. Heat Mass Transf. 143 (2019) 118570.